Journal of Controlled Release 379 (2025) 327–343

Contents lists available at ScienceDirect

Journal of Controlled Release

journal homepage: www.elsevier.com/locate/jconrel

Co-activating STING-TLR9 pathways promotes radiotherapy-induced cancer vaccination

Yu Sun [a], Liang Liu [a,b], Huilan He [a], Guanhong Cui [a], Yun Zheng [a], Chunlian Ye [a], Liping Qu [a], Yinping Sun [a], Jinlong Ji [a], Twan Lammers [c], Ying Zhang [a,*], Zhiyuan Zhong [a,*]

[a] College of Pharmaceutical Sciences, College of Chemistry, Chemical Engineering and Materials Science, Soochow University, Suzhou 215123, People's Republic of China; State Key Laboratory of Radiation Medicine and Protection, Soochow University, Suzhou 215123, People's Republic of China
[b] School of Optical and Electronic Information, Suzhou City University, Suzhou 215104, People's Republic of China
[c] Department of Nanomedicine and Theranostics, Institute for Experimental Molecular Imaging, Helmholtz Institute for Biomedical Engineering, RWTH Aachen University Clinic, Aachen 52074, Germany

ARTICLE INFO

Keywords:
In situ cancer vaccine
Cancer therapy
Nano-agonist
Radiation doses
Immunomodulation

ABSTRACT

Vaccination may cure cancer patients by inducing tumor-specific immune responses. Radiotherapy is an appealing strategy to generate cancer vaccines in situ; thus far, however, only modest and short-lived immune responses are achieved. We here show that radiation combined with co-activating STING-TLR9 can generate powerful in situ cancer vaccines. Notably, radiation at a dose of 12 Gy is found to be optimal for boosting tumor cell immunogenicity, and STING-TLR9 co-stimulation by a dual immune activation nano-agonist overrides key immunosuppressive effects associated with radiotherapy. Local radiotherapy combined with the dual immune activation nano-agonists elicits strong systemic anti-tumor immune responses, resulting in complete regression of tumors and metastases in multiple syngeneic murine tumor models. This work introduces a novel and highly potent cancer immunotherapeutic strategy that holds promise for the personalized treatment of intractable cancers.

1. Introduction

Immunotherapy has emerged a mainstay of modern clinical cancer treatment [1–4]. Cancer vaccines are immunotherapeutic strategies designed to eradicate tumor cells by enabling the host immune systems with tumor-specific killing effects, demonstrating promising potential in both prophylactic and therapeutic cancer settings [5,6]. However, the development of protein/peptide vaccines and mRNA vaccines generally relies on pre-identified tumor antigens or their sequences, thus may be impeded by the intricate and time-intensive processes required for the identification and production of tumor antigens [7,8]. Moreover, given the complex heterogeneity of solid tumor tissues and the potential neoantigen mutation in tumor cells, these cancer vaccines based on pre-identified tumor antigens may yield suboptimal outcomes due to insufficient targeting of diverse tumor antigens [7,9]. In situ cancer vaccines offer a potential solution to these challenges by converting a patient's own tumor into a source for the presentation of a diverse array of tumor-specific antigens, thus stimulating a broad and effective anti-tumor T cell response [10,11].

As an integral component of clinical cancer treatment, radiotherapy (RT) has demonstrated in situ vaccination effects in both pre-clinical and clinical studies [12–14]. Despite these promising findings, it has also indicated that the in situ cancer vaccination elicited by RT alone is modest for complete tumor eradication, especially for immunologically "cold" tumors [15–17]. This can be ascribed to the multifaceted effects of RT in modulating both the immunogenicity and immunosuppression of solid tumor tissues. Radiation initiates cascaded cellular signals, induces immunogenic cell death (ICD) of tumor cells, and primes a potent type-I interferon (IFN-I) immune response in both tumor cells and stroma cells. Through these mechanisms, radiation not only stimulates innate and adaptive anti-tumor immune responses but also regulates the influx of immune cells [18–20]. Moreover, investigations have revealed that RT can directly re-orchestrate the immune constitution of tumors by inducing a transient depletion of tumor-infiltrating lymphocytes due to their high radiosensitivity and modulating the polarization of immune cells (e.g., macrophages and helper T cells) [21–25]. These suggest the

* Corresponding authors at: College of Pharmaceutical Sciences, College of Chemistry, Chemical Engineering and Materials Science, Soochow University, Suzhou 215123, People's Republic of China.
E-mail addresses: yzhang628@suda.edu.cn (Y. Zhang), zyzhong@suda.edu.cn (Z. Zhong).

https://doi.org/10.1016/j.jconrel.2024.12.079
Received 8 November 2024; Received in revised form 18 December 2024; Accepted 31 December 2024
Available online 14 January 2025

paradoxical immunomodulatory effects of RT, which however are critical in the development of in situ cancer vaccines. To enhance the efficacy of radio-immunotherapy by mitigating tumor immunosuppression, various strategies have been developed, include reprogramming the tumor metabolic microenvironment by inhibiting indoleamine 2,3-dioxygenase 1 (IDO-1), blocking immunosuppressive pathways such as CD73, and depleting immunosuppressive myeloid cells using small molecular inhibitors [26–28]. However, despite these advances, the intricate interplay between radiotherapy doses and cancer immunotherapy remains incompletely understood.

We hypothesize that the multifaceted modulatory effects of RT are closely associated with the radiation dose. In this study, we therefore sought to develop a high-efficacy in situ cancer vaccination strategy by optimizing the RT dose to increase tumor immunogenicity and constructing a dual immune activation nano-agonist (CAP: *co*-loaded CpG ODN and ADU-S100 polymersomes) to target STING-TLR9 pathways for specifically overcoming the immunosuppressive effects that RT exerts on macrophages and T cells (Scheme 1). We demonstrate a relationship between the multifaceted modulatory effects of RT and radiation dose. Since CAP potently reversed the immunosuppressive responses induced by RT (e.g., M2 macrophages, Th2/Tc2 cells), the in situ cancer vaccination generated by RT at an optimized dose and CAP elicited a robust anti-tumor immune response with abscopal effects, eradicating localized tumors and preventing lung metastasis. By optimizing the radiation dose to augment tumor immunogenicity and specifically antagonizing its adverse immunoregulatory effects via a purposefully developed dual immune activation nano-agonist, this approach provides a straightforward solution to achieve robust in situ cancer vaccination.

2. Materials and methods

2.1. Materials

CpG ODN 1826 (CpG, 5'-TCCATGACGTTCCTGACGTT-3') was purchased from Sangon Biotech. ADU-S100 (CAS.1638241-89-0) was purchased from MedChemExpress (MCE). Mouse IL-12p70 ELISA kit (cat. 88-7121-88), mouse IL-1β ELISA kit (cat. 88-7013-88) and mouse IL-6 ELISA kit (cat. 88-7064-88) were purchased from Thermo Fisher and used according to the manufacturer's instructions. Granulocyte-macrophage colony stimulating factor (GM-CSF, cat. 315-03) and macrophage colony stimulating factor (M-CSF, cat. 315-02) were purchased from PeproTech. Enhanced ATP assay kit (cat. S0027) was purchased from Beyotime Biotechnology and used according to the manufacturer's instructions. Annexin V-APC/7-AAD apoptosis kit (cat. AP105-100) was purchased from Multi Sciences. RNA-easy isolation reagent (cat. R701-02), HiScript lll RT SuperMix for qPCR (+gDNA wiper) (cat. R323-01) and Taq Pro universal SYBR qPCR master mix (cat. Q712-02) were purchased from Vazyme. The sequences of the primers used for RT-qPCR and the information of antibodies and markers used in this study are provided in Table S1 and Table S2 in the Supplementary material, respectively.

2.2. Cell lines and animals

4T1 cells were obtained from the Type Culture Collection of the Chinese Academy of Sciences (Shanghai, China), and 4T1-Luc cells were obtained from Fuheng Biotechnology (Shanghai, China). They were all

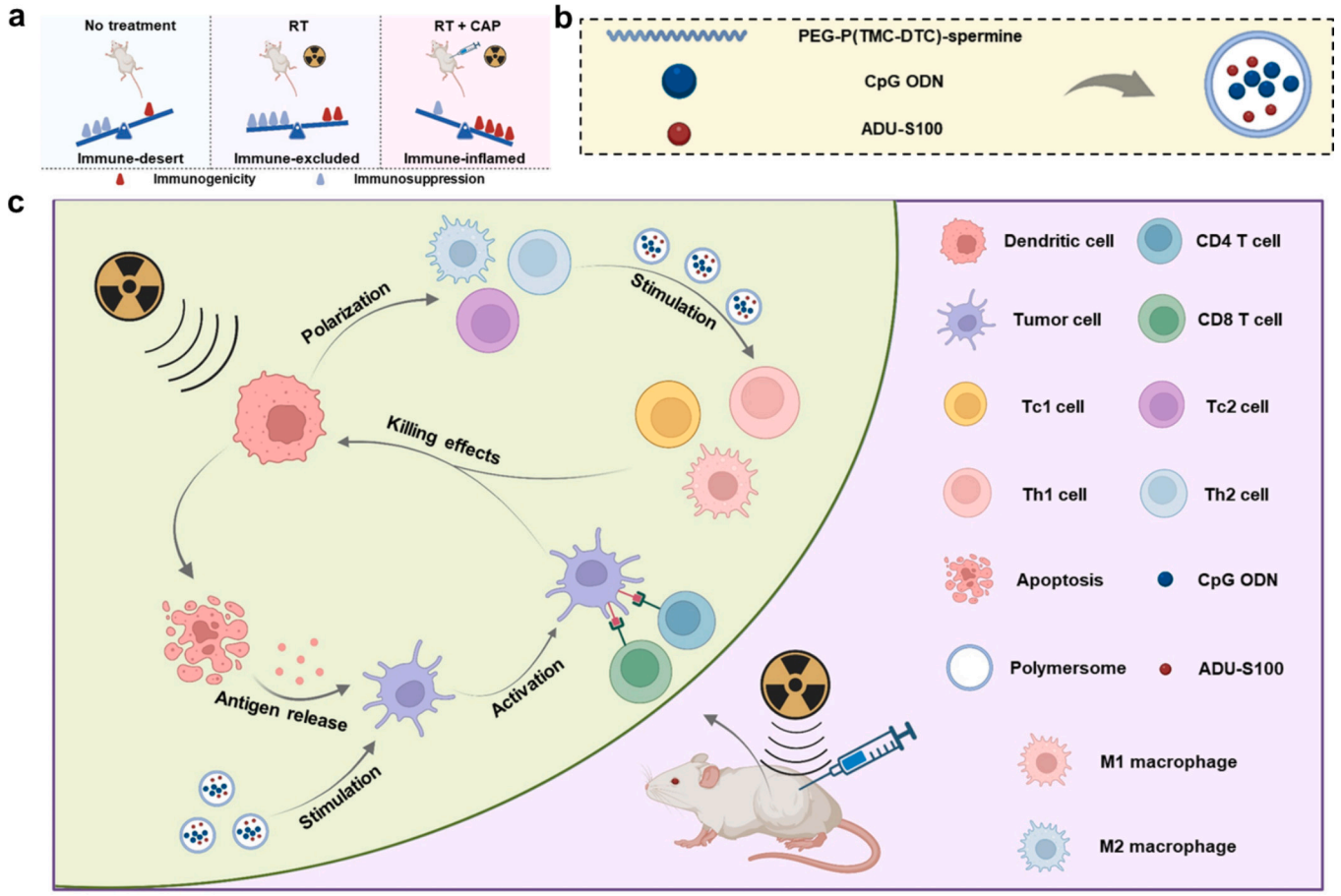

Scheme 1. Preparation and proposed mechanism of CAP in potentiating the in situ vaccination effects of RT. (a) A summary of the immunomodulatory effects of RT and RT + CAP. (b) Schematic illustration of the preparation of CAP. (c) Schematic presentation of the effects of RT and CAP in eliciting an in situ cancer vaccine. This figure was created with Biorender.com.

cultured in RPMI-1640 medium. B16-F10 cells and 293T cells were obtained from the American Type Culture Collection (ATCC) and cultured in DMEM. HeLa cells were obtained from ATCC and cultured in RPMI-1640 medium. RAW264.7 macrophages were obtained from the National Collection of Authenticated Cell Cultures and cultured in DMEM. All the cell culture media were supplemented with 10 % FBS, 1 % penicillin and 1 % streptomycin.

Bone marrow-derived dendritic cells (BMDCs) and bone marrow-derived macrophages (BMDMs) were derived from the bone marrow of C57BL/6 mice (6–7 weeks, female, 18–20 g, Slac). BMDCs and BMDMs were cultured in RPMI-1640 medium supplemented with 10 % FBS, 1 % penicillin and 1 % streptomycin. The culture medium was supplemented with 20 ng/mL recombinant mouse GM-CSF or 25 ng/mL recombinant mouse M-CSF for the culture of BMDCs and BMDMs, respectively. To isolate mouse splenocytes, spleens were collected from C57BL/6 mice aseptically and dissociated into single-cell suspensions. After lysing red blood cells (RBCs) using ACK lysis buffer, the splenocytes were re-suspended and cultured in RPMI-1640 medium supplemented with 10 % FBS, 1 % penicillin and 1 % streptomycin for further use.

Female C57BL/6 mice (6–8 weeks) were purchased from Slac Animal Company (Shanghai, China). Female BALB/c mice (6–8 weeks) were purchased from Vital River Animal Company (Beijing, China). All animal experiments were approved by the Animal Care and Use Committee of Soochow University, and all protocols conformed to the Guide for the Care and Use of Laboratory Animals.

2.3. Synthesis and characterization of CAP, CP and AP

Poly(ethylene glycol)-*b*-poly(trimethylene carbonate-*co*-dithiolane trimethylene carbonate)-spermine (PEG-P(TMC-DTC)-spermine) was synthesized as reported previously [29,30]. To construct CAP, CP and AP, 30 μL *N*,*N*-dimethylformamide (DMF) containing PEG-P(TMC-DTC)-spermine (40 mg/mL) was added into phosphate buffer (pH 6.0, 300 μL) containing ADU-S100 (0.2 mg/mL) and/or CpG (0.4 mg/mL) under stirring at 300 rpm. After stirring at room temperature for 10 min, the dispersion was transferred to a dialysis tubing (MWCO: 350 kDa) and dialyzed against phosphate buffer (pH 6.0, 2 L) for 3 h and then phosphate buffer (pH 7.4, 2 L) for 2 h to remove DMF and the unencapsulated CpG and ADU-S100. The hydrodynamic diameters of CAP, CP and AP were characterized by a dynamic light scattering (DLS) spectrometer (Malvern Zetasizer Nano ZS) with a sample concentration of 0.1 mg/mL. The amounts of CpG and ADU-S100 loaded in CAP, CP and AP were determined by a Nanodrop One Microvolume UV–Vis Spectrophotometer (Thermo Scientific). The drug loading efficiencies (DLEs) of CpG and ADU-S100 were calculated based on the following formula:

$$\text{DLE (wt\%)} = \text{weight of immune agonist loaded/weight of immune agonist in feed} \times 100\ (\%)$$

2.4. Cytotoxicity of polymersome

The cytotoxicity of the polymersome fabricated from PEG-P(TMC-DTC)-spermine was evaluated in 4T1 cells, RAW264.7 macrophages and 293T cells. 4T1 cells and RAW264.7 macrophages were seeded in 96-well plates (3×10^3 cells/well). 293T cells were seeded in 96-well plates (5×10^3 cells/well). The cells were incubated overnight. Polymersome with different concentrations was added to the cells and incubated for 24 h. MTT solution was added to the cells at a final concentration of 0.5 mg/mL. After 4 h of incubation, the culture medium was discarded and 100 μL DMSO was added to each well to dissolve the formazan crystal. Absorbance was measured at 570 nm using a plate reader. Cell viability was calculated using the following equation: Cell viability (%) = $\text{Absorbance}_{(\text{sample})}/\text{Absorbance}_{(\text{PBS})} \times 100$ %.

2.5. Effects of radiation on tumor cells in vitro

4T1 cells and B16F10 cells were seeded in 12-well plates (10^5 cells/well) and incubated overnight. External beam X-ray radiation (RS-2000Pro, Red source) at different doses (0 Gy, 3 Gy, 12 Gy, 20 Gy) was applied to these cells. The culture medium was replaced with fresh medium after radiation. 24 h later, the culture medium was collected for the quantitative analysis of ATP using an enhanced ATP assay kit according to the manufacturer's instructions, and the cells were collected for the evaluation of CRT expression. The irradiated cells were stained with an anti-calreticulin-ER antibody for 1 h, followed by washing with cold PBS twice and staining with an Alexa 647-conjugated secondary antibody for 30 min. Flow cytometry analyses of these cells were performed on a BD FACSVerse flow cytometer. To study the effects of radiation at different doses on the apoptosis of tumor cells, 4T1 cells and B16F10 cells were collected at 24 h post-irradiation and stained with an Annexin V-APC/7-AAD apoptosis kit according to the manufacturer's instructions. Flow cytometry analyses of these cells were performed on a BD FACSVerse flow cytometer. To evaluate the levels of immune cytokines derived from irradiated tumor cells, 4T1 cells, B16F10 cells and HeLa cells were collected at 48 h post-irradiation. RNA was isolated from these cells using an RNA-easy isolation reagent according to the manufacturer's instructions. Then, cDNA was synthesized using an HiScript lll RT SuperMix for qPCR (+gDNA wiper) according to the manufacturer's protocol. Quantitative PCR was performed using a Taq Pro universal SYBR qPCR master mix to study the expression of *Ifnβ*, *Cxcl10* and *Tnfα*. Thermal cycling conditions included: 95 °C for 2 min (denaturation), followed by 40 cycles of 95 °C for 5 s and 60 °C for 30 s (annealing/extension). The mRNA levels of target genes were normalized to the levels of *Hprt* using the $2^{-\Delta\Delta Cq}$ method. Each experiment was repeated three times.

2.6. Effects of radiation on immune cells in vitro

To study the effects of radiation on macrophages in vitro, BMDMs were seeded in 6-well plates (10^6 cells/well) and incubated overnight. External beam X-ray radiation at different doses (0 Gy, 3 Gy, 12 Gy, and 20 Gy) was applied to these cells. The culture medium was replaced with fresh medium after radiation. 24 h later, the cells were collected and stained with live/dead Zombie NIR. After being incubated with anti-CD16/32 and washed with FACS buffer, the cells were stained with anti-CD206-Alexa 647, anti-F4/80-PE, anti-CD11b-FITC, and anti-CD86-PE/Cy7. Flow cytometry analyses of these cells were performed on a BD FACSVerse flow cytometer.

To study the effects of radiation-primed tumor cell metabolites on the functions of T cells, 4T1 cells and B16F10 cells were seeded in 12-well plates (1×10^5/well) and incubated overnight. External beam X-ray radiation at different doses (0 Gy, 3 Gy, 12 Gy, and 20 Gy) was applied to these cells. The culture medium was replaced with fresh medium after radiation. 24 h later, culture medium was collected from the irradiated cells and added to fresh splenocytes pre-seeded in 6-well plates at a density of 6×10^6 cells/well. The final culture medium for splenocytes consisted of 50 % radiation-primed medium from tumor cells and 50 % fresh cell culture medium. After 24 h of incubation, the

splenocytes were collected. RNA was isolated from these cells, and RT-qPCR was performed according to the methods described above to analyze the expression of *Ifnγ* and *Il4* in these splenocytes.

2.7. Immunomodulatory effects of CAP and 12 Gy radiation on immune cells

BMDMs were seeded in 6-well plates (10^6 cells/well) and incubated overnight. External beam X-ray radiation at 12 Gy was applied to these cells. After radiation, the culture medium was replaced with fresh medium, followed by the addition of CAP (CpG: 1.2 μg/mL; ADU-S100: 0.3 μg/mL). 24 h later, the cells were collected and stained with live/dead Zombie NIR. After being incubated with anti-CD16/32 and washed with FACS buffer, the cells were stained with anti-CD206-Alexa 647, anti-F4/80-PE, anti-CD11b-FITC, and anti-CD86-PE/Cy7. Flow cytometry analyses of these cells were performed on a BD FACSVerse flow cytometer.

RAW264.7 macrophages were seeded in 12-well plates (3×10^5 cells/well) and incubated overnight. External beam X-ray radiation at 12 Gy was applied to these cells. After radiation, the culture medium was replaced with fresh medium, followed by the addition of CAP (CpG: 1.2 μg/mL; ADU-S100: 0.3 μg/mL). 24 h later, the cells were collected. RNA was isolated from these cells, and RT-qPCR was performed according to the methods mentioned above to analyze the expression of *Nos2* and *Arg1* in these cells.

Fresh splenocytes were seeded in 6-well plates (6×10^6 cells/well) and cultured with 50 % cell culture medium collected from 12 Gy-irradiated 4T1 cells or B16F10 cells at 24 h post-irradiation. CAP (CpG: 1.2 μg/mL; ADU-S100: 0.3 μg/mL) was added to the cells. 24 h later, splenocytes were collected. RNA was isolated from these cells, and RT-qPCR was performed according to the methods described above to analyze the expression of *Ifnγ* and *Il4* in these splenocytes.

2.8. Immunomodulatory effects of CAP, CP and AP in vitro

To study the effects of CAP, CP and AP on the activation of dendritic cells (DCs), BMDCs were seeded in 12-well plates (1×10^6/well) and incubated overnight. CAP (CpG: 1.2 μg/mL, ADU-S100: 0.3 μg/mL), CP (CpG: 1.2 μg/mL) or AP (ADU-S100: 0.3 μg/mL) was added to the cells. 24 h later, the culture medium was collected for the analyses of IL-12p70 and IL-1β using corresponding mouse ELISA kits, and the cells were stained with live/dead Zombie NIR. After incubation with anti-CD16/32 and washing with FACS buffer, the cells were stained with anti-CD11c-FITC, anti-CD80-APC and anti-CD86-PE. Flow cytometry analyses of BMDCs were performed on a BD FACSVerse flow cytometer.

To study the immunomodulatory effects of CAP, CP and AP on irradiated macrophages, RAW264.7 macrophages were seeded in 6-well plates (3×10^5/well) and incubated overnight. External beam X-ray radiation at 12 Gy was applied to the cells. The culture medium was replaced with fresh medium after radiation. CAP (CpG: 1.2 μg/mL, ADU-S100: 0.3 μg/mL), CP (CpG: 1.2 μg/mL) or AP (ADU-S100: 0.3 μg/mL) was added to the cells. After incubation for another 4 h, the cells were collected. RNA was isolated from these cells, and RT-qPCR was performed according to the methods described above to analyze the expression of *Ifnβ*, *Arg1* and *Nos2* in these cells.

2.9. Therapeutic performance of CAP + 12 Gy RT treatment in murine tumor models

To establish 4T1 breast tumor-bearing mice, BALB/c mice were inoculated subcutaneously with 2×10^5 4T1 cells/mouse on the right flank. To establish B16F10 melanoma-bearing mice, C57BL/6 mice were inoculated subcutaneously with 2×10^5 B16-F10 cells/mouse on the right flank. To establish 4T1 two tumor-bearing mice, BALB/c mice were inoculated subcutaneously with 2×10^5 4T1 cells/mouse on the right flank and 2×10^5 4T1 cells/mouse on the left flank five days later. Once the volume of tumors (primary tumors on the right flank for 4T1 two tumor-bearing mice) reached 80–100 mm^3, mice were randomized, and treatment began. When the tumor volume reached ~2000 mm^3, mice were euthanized. The diameter of the tumors was measured every three days, and tumor volume was calculated according to the following equation: tumor volume = long diameter × short diameter^2 × 0.5.

On treatment day 0, 12 Gy of external beam X-ray radiation was applied to the tumor region. 6 h later, 50 μL aqueous suspension containing CAP (CpG: 20 μg; ADU-S100: 5 μg), CP (CpG: 20 μg) or AP (ADU-S100: 5 μg) was intratumorally injected. The intratumoral administration of these formulations at the same doses was performed on days 3, 6, and 9 thereafter.

2.10. Immune response generated by CAP + 12 Gy RT treatment in murine tumor models

4T1 breast tumor-bearing mice were established and treatment was performed as described above. The mice were euthanized on day 12 post-initiation of treatment, and the spleens and blood were collected from these mice. The spleens were dissociated into single-cell suspensions. After the RBCs were lysed using ACK lysis buffer, the splenocytes were stained with live/dead Zombie NIR, incubated with anti-CD16/32 and washed with FACS buffer. Then, the splenocytes were divided into groups for CD4 T cell staining and CD8 T cell staining separately. For CD4 T cell staining, the splenocytes were stained with anti-CD45-PE, anti-CD3-FITC, anti-CD4-PE/Cy7, anti-CD44-PerCP/Cy5.5 and anti-IFNγ-APC. For CD8 T cell staining, the splenocytes were stained with anti-CD45-PE, anti-CD3-FITC, anti-CD8a-PE/Cy7, anti-CD44-PerCP/Cy5.5 and anti-IFNγ-APC. Flow cytometry analyses of these splenocytes were performed on a BD FACSVerse flow cytometer. To collect blood cells, RBCs were lysed using ACK lysis buffer. Subsequently, the blood cells were stained with live/dead Zombie NIR, incubated with anti-CD16/32 and washed with FACS buffer. Then, the blood cells were divided for CD4 T cell staining and CD8 T cell staining separately. For CD4 T cell staining, blood cells were stained with anti-CD45-PerCP/Cy5.5, anti-CD4-PE, anti-CD3-PE/Cy7 and anti-IFNγ-APC. For CD8 T cell staining, blood cells were stained with anti-CD45-PE, anti-CD3-PE/Cy7, anti-CD8a-FITC and anti-IFNγ-APC. Flow cytometry analyses of these blood cells were performed on a BD FACSVerse flow cytometer.

B16F10 melanoma-bearing mice were established and treatment was performed as described above. Blood was collected from these mice 6 h after the intratumoral injection of CAP on day 6 since the initiation of treatment. The levels of IL-6 and IL-12p70 in the serum were determined by the corresponding mouse ELISA kits.

2.11. Systemic immunity and immune memory generated by CAP + 12 Gy RT treatment

4T1 breast tumor-bearing mice were established and treatment was performed as described above. Blood was collected from these mice on day 15 post-initiation of treatment. RBCs were lysed using ACK lysis buffer. Subsequently, the blood cells were stained with live/dead Zombie NIR, incubated with anti-CD16/32 and washed with FACS buffer. Then, the splenocytes were stained with anti-CD45-APC, anti-CD3-FITC, anti-CD4-PE and anti-CD8a-PE/Cy7. Flow cytometry analyses of these blood cells were performed on a BD FACSVerse flow cytometer.

On day 28 post-initiation of treatment, the mice in the CAP +12 Gy RT treatment group were inoculated with 2×10^5 4T1 cells/mouse on the contralateral side. A group of age-matched naive mice were also engrafted with 2×10^5 4T1 cells for tumor growth as a control. On day 42 post-initiation of treatment, the mice were euthanized. Spleens and re-challenged tumor tissues were collected from euthanized mice and dissociated into single-cell suspensions. The RBCs in splenocytes were lysed using ACK lysis buffer. All the single-cell suspensions were stained with live/dead Zombie NIR, incubated with anti-CD16/32 and washed

with FACS buffer. Then, the splenocytes were divided into groups for CD4 T cell staining and CD8 T cell staining separately. For CD4 T cell staining, the splenocytes were stained with anti-CD45-APC, anti-CD3-FITC, anti-CD4-PE/Cy7, anti-CD62L-PE and anti-CD44-PerCP/Cy5.5. For CD8 T cell staining, the splenocytes were stained with anti-CD45-APC, anti-CD3-FITC, anti-CD8a-PE/Cy7, anti-CD62L-PE and anti-CD44-PerCP/Cy5.5. Tumor cells were stained with anti-CD45-APC, anti-CD3-FITC, anti-CD4-PE, anti-CD8a-PE/Cy7 and anti-NK1.1-PerCP/Cy5.5. Flow cytometry analyses of splenocytes and tumor cells were performed on a BD FACSVerse flow cytometer.

2.12. Effects of CAP + 12 Gy RT treatment against postoperative tumor recurrence

To establish a postoperative tumor recurrence model, BALB/c mice were inoculated subcutaneously with 2×10^5 4T1 cells/mouse on the right flank. Once the tumor volumes reached 200–300 mm^3, 95 % of the tumor volume was resected. Tumor recurrence occurred after surgical resection. When the volume of the recurrent tumors reached 150 mm^3, mice were randomized and treatment as described above was started. The whole body of the mice was scanned with an in vivo imaging system (IVIS, Lumina, PE). The tumor growth of the mice was monitored as described above.

2.13. Statistical analysis

The data are presented as mean ± standard deviation (SD). The significant differences among groups were determined using GraphPad Prism 8 by one-way ANOVA (Tukey multiple comparison tests) or an unpaired *t*-test (for two-group comparisons only). The survival rate of the mice was analyzed by Kaplan-Meier technique with a log-rank test for comparison. $^*p < 0.05$, $^{**}p < 0.01$, $^{***}p < 0.001$ and $^{****}p < 0.0001$.

3. Results

3.1. Radiation increases the immunogenicity of tumor cells but also induces immunosuppressive responses

One of the central aims of this study is to investigate the relationship between radiation dose and its immunomodulatory effects, and to develop strategies to counteract the adverse immunoregulatory effects of radiation at the optimal immunostimulatory dose, thereby providing a robust in situ cancer vaccine. Currently, clinical RT regimens are diverse. For example, RT is conventionally given in a hyper-fractionated manner, at small daily doses (~1–3 Gy), with total doses eventually going up to 60–80 Gy [31]. Recent advances in radiation techniques, such as stereotactic ablative radiotherapy and stereotactic body radiotherapy, have enabled a shift to hypo-fractionated radiation that employs larger or ablative doses of approximately 5–24 Gy per fraction with shorter treatment schedules [31,32]. In this study, we selected three doses of radiation (3 Gy, 12 Gy, 20 Gy) that are widely used in clinical practice and aimed to evaluate their multifaceted modulatory effects on both tumor cells and immune cells [33–35].

Immunologically "cold" murine triple-negative 4T1 breast tumors were used in this study. As illustrated in Fig. S1, analyses of bulk tumor samples revealed that 4T1 solid tumors mainly comprise $CD45^-$ tumor or stromal cells with a minor proportion of infiltrating $CD45^+$ immune cells. While immune cells are commonly recognized as professional responders to external or internal stimuli and modulators of the immune microenvironment of solid tumors, emerging evidence suggests that cancer cells that predominate in solid tumors may also play important roles in the immune microenvironment of tumor tissues by directly or indirectly interacting with immune cells [36,37]. Therefore, we initially studied the immunomodulatory effects of RT at different doses on tumor cells. By analyzing the apoptosis of irradiated 4T1 cells, we found 12 Gy and 20 Gy were more effective than 3 Gy in inducing both early apoptosis and immunogenic late apoptosis/secondary necrosis (Fig. 1a-1b). Further evaluations on the expression of calreticulin (CRT) on irradiated 4T1 cells revealed that both 12 Gy and 20 Gy irradiation effectively induced ICD of 4T1 cells, while 3 Gy irradiation had negligible effects on CRT expression (Fig. 1c and S2). Subsequently, we assessed the production of multiple immune cytokines by tumor cells following irradiation. We found that the expression of *Ifnβ1*, a representative IFN-I and marker of cGAS-STING signaling pathway activation, was significantly higher in 4T1 cells upon 12 Gy irradiation compared to both untreated control cells and cells irradiated with 3 Gy or 20 Gy (Fig. 1d) [38]. CXCL10 is a chemokine that can attract T lymphocytes and is produced downstream of IFN-I after cGAS-STING activation, while TNF*α* is a cytokine that is secreted during the acute inflammation stage and is important for modulating the innate immune response [39,40]. By further examining mRNA expression in irradiated 4T1 cells, we observed a notable increase in the expression of *Cxcl10* and *Tnfα* in the 12 Gy irradiated group (Fig. 1d).

Due to the abundance of $CD11b^+$ myeloid cells among the immune cells infiltrating in 4T1 solid tumors (Fig. S1), we investigated the effects of radiation dose on the polarization of macrophages, a critical myeloid lineage in tumor immunomodulation [41]. Bone marrow-derived macrophages (BMDMs) were isolated from C57BL/6 mice and irradiated with doses of 3 Gy, 12 Gy or 20 Gy (Fig. 1e). As depicted in Fig. 1f-1g, we observed that radiation effectively skewed BMDMs toward the $CD206^+$ M2 phenotype in a dose-dependent manner, potentially attenuating the anti-tumor immune response elicited by RT.

Although a prominent feature of immunologically "cold" tumors is the limited pre-infiltration of effector T lymphocytes (Fig. S1), RT-induced CXCL10 may function as a T cell attractant [42]. Therefore, it would be valuable to evaluate how these cells can be promptly re-educated by RT-primed signals. For this, we collected the supernatants of irradiated 4T1 cells and co-cultured them with splenocytes harvested from naive C57BL/6 mice (Fig. 1h). RT-qPCR analyses revealed a significantly decrease in the expression ratios of *Ifnγ*:*Il4* in splenocytes after co-culture with the supernatants of irradiated 4T1 cells, indicating a bias of T cells toward a Th2/Tc2 phenotype, which may dampen the adaptive cellular immune response induced by RT (Fig. 1i) [43]. Based on these results, although 12 Gy radiation is optimal for enhancing the immunogenicity of tumor cells, its adverse immunomodulatory effects on macrophages and T cells may impede its in situ cancer vaccination effects (Fig. 1j).

3.2. Co-activating STING-TLR9 pathways antagonizes radiotherapy-induced immunosuppression

Immune agonists have been widely developed to target cellular signaling pathways and exhibit various immunomodulatory effects. A simultaneous activation of dual or multiple signaling pathways within the same cells may enhance and diversify the immune response [44–46]. In order to achieve a robust in situ cancer vaccine using RT, we developed a co-activating STING-TLR9 (CAST) strategy by a nano-agonist CAP to mitigate the adverse immunosuppression on macrophages and T cells induced by 12 Gy RT. CAP with a uniform diameter of approximately 50 nm was fabricated by *co*-delivering the TLR9 agonist CpG ODN (CpG) and the cGAS-STING agonist ADU-S100 into a biodegradable polymersome with negligible cytotoxicity (Fig. S3-S5). Due to the distinct signaling pathways targeted, the integration of CpG with ADU-S100 potentially elicits robust innate immune stimulation and polarizes macrophages and T cells [47]. We assessed the immunomodulatory effects of CAP in vitro. As shown in Fig. 2a-2d, increased M1:M2 macrophage ratios among BMDMs and elevated *Nos2*:*Arg1* expression ratios in RAW264.7 macrophages were observed after CAP incubation, indicating CAP's ability to polarize macrophages toward the M1 phenotype. Furthermore, CAP significantly increased the expression ratio of *Ifnγ*:*Il4* in splenocytes, indicating Th1/Tc1 polarization of T cells and enhanced

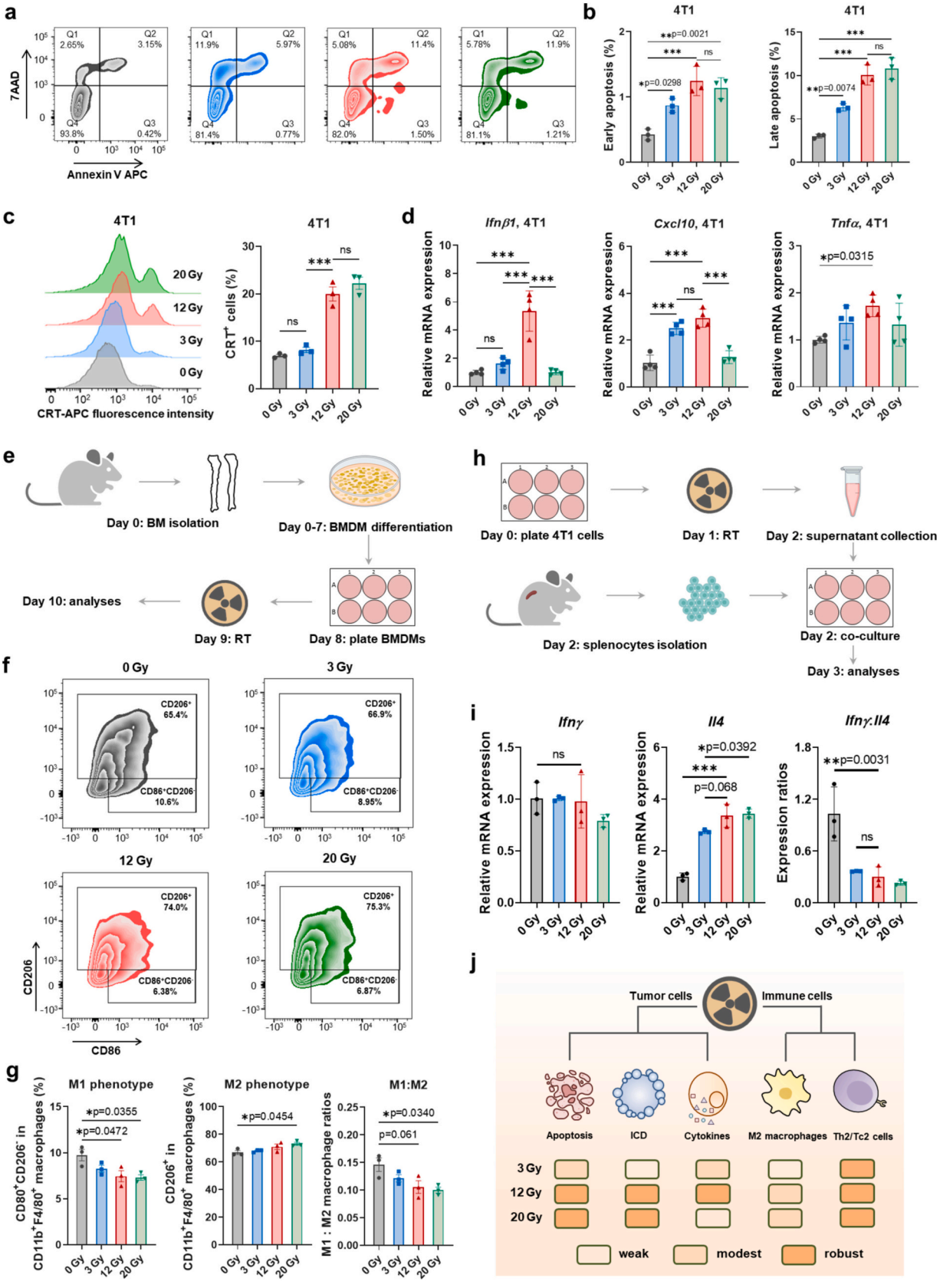

(caption on next page)

Fig. 1. The multifaceted modulatory effects of radiation on tumor cells and immune cells are dose-dependent. (a) Representative flow cytometry analysis of the apoptosis and (b) percentages of early apoptosis and late apoptosis among 4T1 cells at 24 h after irradiation at different doses ($n = 3$). (c) Histogram graphs of CRT expression on 4T1 cells and percentages of CRT^+ 4T1 cells at 24 h after irradiation at different doses ($n = 3$). (d) Relative expression of *Ifnβ1*, *Cxcl10* and *Tnfα* in 4T1 cells at 48 h after irradiation at different doses ($n = 4$). (e) Schematic illustration of the study of macrophage polarization upon irradiation. BM: bone marrow. (f) Representative flow cytometry analysis of irradiated BMDMs. (g) Percentages of the M1 phenotype ($CD86^+CD206^-$) and M2 phenotype ($CD206^+$) among $CD11b^+F4/80^+$ BMDMs and the ratios between M1 and M2 macrophages at 24 h after irradiation at different doses (n = 3). (h) Schematic illustration of the study of radiation-primed cues on T cell function. (i) Relative expression of *Ifnγ* and *Il4* and expression ratios of *Ifnγ:Il4* in splenocytes at 24 h after co-culture with supernatants collected from irradiated 4T1 cells (n = 3). (j) A brief summary about the multifaceted modulatory effects of radiation with different doses on 4T1 tumor cells and immune cells (ICD: immunogenic cell death). Statistical significance was calculated via one-way ANOVA test in b-d, g and i. The data are presented as mean ± SD. $^*p < 0.05$, $^{**}p < 0.01$, $^{***}p < 0.001$.

tumor-killing effects of lymphocytes generated by CAP (Fig. 2e-2f). Considering the immunosuppression induced by radiation, we subsequently evaluated CAP's ability to reverse these adverse immune polarizations on both macrophages and T cells. By incubating 12 Gy-irradiated BMDMs with CAP, we observed a significant increase in the levels of M1-polarized cells, which was further confirmed by the elevation in the *Nos2:Arg1* expression ratio in 12 Gy-irradiated RAW264.7 macrophages upon CAP treatment (Fig. 2a, c, g-2h). To test CAP's effects on relieving the Th2/Tc2 polarization of T cells induced by radiation-primed cues, we added CAP to a co-culture system of splenocytes with supernatants collected from irradiated 4T1 cells (Fig. 2e). We found that CAP significantly increased the expression ratio of *Ifnγ:Il4* in splenocytes, indicating that the Th1/Tc1 polarization of T cells recovered to support a potent anti-tumor immune response (Fig. 2i).

3.3. Dual immune activation nano-agonist potentiates radiotherapy-induced in situ vaccination

Given the remarkable ability of CAP to reverse the adverse M2 polarization of macrophages and Th2/Tc2 polarization of T cells induced by 12 Gy RT, we then investigated the potential effects of CAP to potentiate the in situ vaccination effects of RT in vivo. For this purpose, we established immunologically "cold" 4T1 tumor-bearing mice and treated them with focal 12 Gy RT with or without intratumoral injection of CAP (Fig. 3a). As shown in Fig. 3b-3c and 3e, we found 12 Gy RT alone exhibited weak suppression of tumor growth, which was significantly enhanced by the intratumoral injection of CAP, resulting in complete tumor eradication in 2 out of 5 mice and prolonged mouse survival in the CAP +12 Gy RT treatment group. During treatment, no significant changes in animal weight were observed between these treatment regimens (Fig. 3d). Subsequently, we assessed whether 12 Gy RT is indispensable for the robust anti-tumor efficacy of the CAP +12 Gy RT treatment regimen. As shown in Fig. S6, although CAP effectively slowed the growth of pre-inoculated 4T1 breast tumors, this effect was inferior to that of the CAP +12 Gy RT treatment regimen. This highlights the necessity of including 12 Gy RT to generate a robust anti-tumor response.

To determine whether CAP +12 Gy RT treatment generated a potent anti-tumor immune response, we repeated this tumor treatment study and sacrificed the mice on day 12 since the initiation of treatment and collected spleen and blood specimens (Fig. 3a). We evaluated the populations of T cells among the spleens and observed a significant increase in the proportions of $CD3^+$ T cells, $CD3^+CD4^+$ T cells and $CD3^+CD8^+$ T cells in the CAP +12 Gy RT treated mice compared to both the untreated control mice and the 12 Gy RT treated mice (Fig. 3f-3h and S7-S8). Furthermore, we investigated the effects of cytotoxic and effector markers on these T cells, and found that the levels of both cytotoxic T cells and effector T cells were higher in the spleens of CAP +12 Gy RT treated mice than in those of untreated control or 12 Gy RT treated mice (Fig. 3f-3g). To study whether CAP +12 Gy RT treatment generated a systemic anti-tumor immune response, we collected blood cells from 4T1 tumor-bearing mice after different treatments and analyzed the cytotoxic markers on circulating T cells. As shown in Fig. 3i, we found that CAP +12 Gy RT treated mice exhibited higher levels of circulating $IFN\gamma^+$ T cells than untreated control mice, and there was a trend toward an increase in this phenotype of T cells in CAP +12 Gy RT treated mice compared to 12 Gy RT treated mice, which may be attributed to $CD8^+$ T cells. We did not observe any apparent histological changes in the normal tissues in these mice, including the liver, kidney, heart or lung, caused by the treatment (Fig. S9). These results indicated that the combination of CAP and 12 Gy RT elicited a robust in situ cancer vaccine.

Subsequently, we examined the necessity of the combination of CpG and ADU-S100 for priming a potent anti-tumor immune response. We formulated CpG and ADU-S100 respectively into the same polymersomes, and the resulting CP (CpG loaded polymersome) and AP (ADU-S100 loaded polymersome) exhibited similar particle size distributions as CAP (Fig. S10). First, we evaluated the effects of CP, AP and CAP on the stimulation of bone marrow-derived dendritic cells (BMDCs). As shown in Fig. 4a-4c, CAP primed the activation ($CD86^+$ and $CD80^+$) of a large proportion of BMDCs, which was significantly greater than that of its single immune activation nano-agonists counterparts (CP and AP) that contained equivalent amounts of CpG or ADU-S100 to that in CAP. By collecting the supernatant of BMDCs, we analyzed the levels of immune cytokines secreted by these cells after different treatments and found that CAP generated greater amounts of both IL-12p70 and IL-1β in BMDCs than did CP or AP (Fig. 4d). Then, we compared the immunomodulatory effects of CP, AP and CAP on irradiated RAW264.7 macrophages. As illustrated in Fig. 4e, CAP was superior to CP and AP in polarizing the irradiated macrophages toward the M1 phenotype and augmenting the expression of *Ifnβ1*. Intriguingly, given the equivalent doses of CpG or ADU-S100 in CAP, CP and AP, we found that AP may perform better than CP in generating co-stimulatory molecules on BMDCs, while CP exhibited stronger effects on the polarization of macrophages than AP. This indicated the potential complementary effects of CpG and ADU-S100 on immunomodulation and necessitated the CAST strategy in augmenting the in situ cancer vaccination effects of 12 Gy RT. Furthermore, we compared the anti-tumor effects of CAP, CP and AP in combination with 12 Gy RT in 4T1 breast tumor-bearing mice (Fig. 4f). We found that although all the treatment regimens, CP + 12 Gy RT, AP + 12 Gy RT and CAP +12 Gy RT, suppressed tumor growth at the early stage of treatment, tumor recurrence and mouse death were observed during long-term monitoring in the CP + 12 Gy RT and AP + 12 Gy RT treatment groups. In contrast, the CAP +12 Gy RT treatment regimen elicited long-lasting tumor growth inhibition, rendering three out of five mice disease-free and prolonging the survival of these mice to at least 180 days since the initiation of treatment (Fig. 4g-4h and 4j). This strongly suggested the significance of CAP, which contains both CpG and ADU-S100, in priming a robust and long-lasting in situ cancer vaccine when coordinated with 12 Gy RT. During the study, no obvious changes were detected in the body weights of mice (Fig. 4i).

3.4. Dual immune activation nano-agonist plus radiotherapy elicits robust in situ cancer vaccination in B16F10 melanoma model

To evaluate the generalizability of the optimized in situ cancer vaccine induced by 12 Gy RT in combination with CAP, we selected another aggressive murine melanoma model B16F10, and examined the efficacy of the CAP +12 Gy RT treatment regimen both in vitro and in vivo. First, we investigated whether 12 Gy irradiation optimally

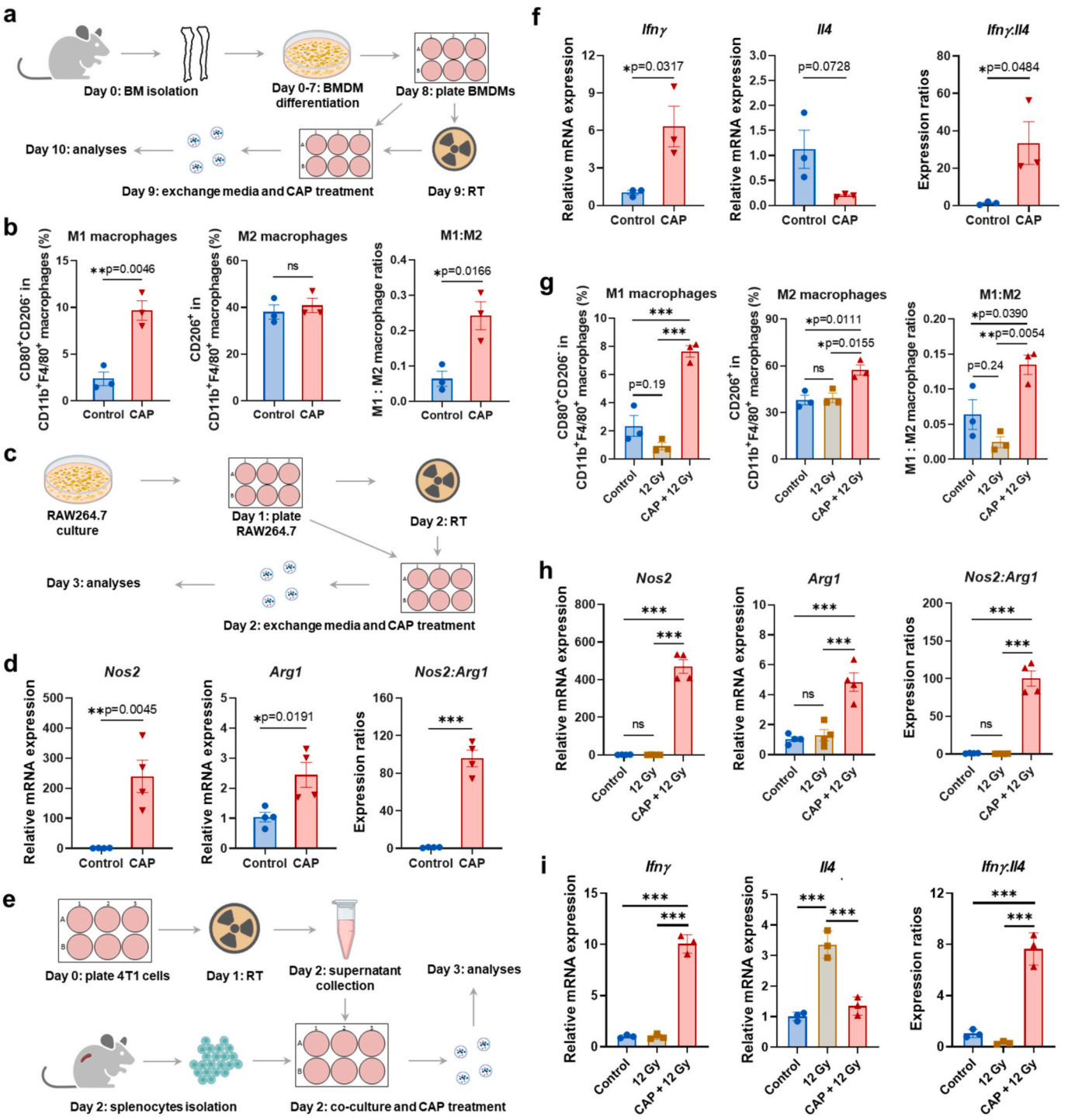

Fig. 2. CAP integrates two immune activation modalities to antagonize the immunoregulatory effects of 12 Gy on macrophages and T cells. (a) Schematic illustration of the study of CAP on macrophage polarization. BM: bone marrow. (b) Percentages of $CD11b^+F4/80^+$ BMDMs with the M1 phenotype ($CD86^+CD206^-$) and M2 phenotype ($CD206^+$) and ratios of M1:M2 macrophages at 24 h after treatment with CAP ($n = 3$). (c) Schematic illustration of the study of CAP on priming *Nos2* and *Arg1* expression in RAW264.7 macrophages. (d) Relative expression of *Nos2* and *Arg1* and expression ratios of *Nos2*:*Arg1* in RAW264.7 macrophages at 24 h after treatment with CAP ($n = 4$). (e) Schematic illustration of the study of CAP on T cell function. (f) Relative expression of *Ifnγ* and *Il4* and expression ratios of *Ifnγ*:*Il4* in splenocytes at 24 h after treatment with CAP (n = 3). (g) Percentages of $CD11b^+F4/80^+$ BMDMs with the M1 phenotype ($CD86^+CD206^-$) and M2 phenotype ($CD206^+$), and the ratios of M1:M2 macrophages at 24 h after the indicated treatment (n = 3). This study was performed according to Fig. 2a. (h) Relative expression of *Nos2* and *Arg1* and expression ratios of *Nos2*:*Arg1* in RAW264.7 macrophages at 24 h after the indicated treatment (n = 4). This study was performed according to Fig. 2c. (i) Relative expression of *Ifnγ* and *Il4* and expression ratios of *Ifnγ*:*Il4* in splenocytes at 24 h after the indicated treatment (n = 3). This study was performed according to Fig. 2e. Statistical significance was calculated via a *t*-test in b, d and f, and one-way ANOVA test in g-i. The data are presented as mean ± SD. $^*p < 0.05$, $^{**}p < 0.01$, $^{***}p < 0.001$.

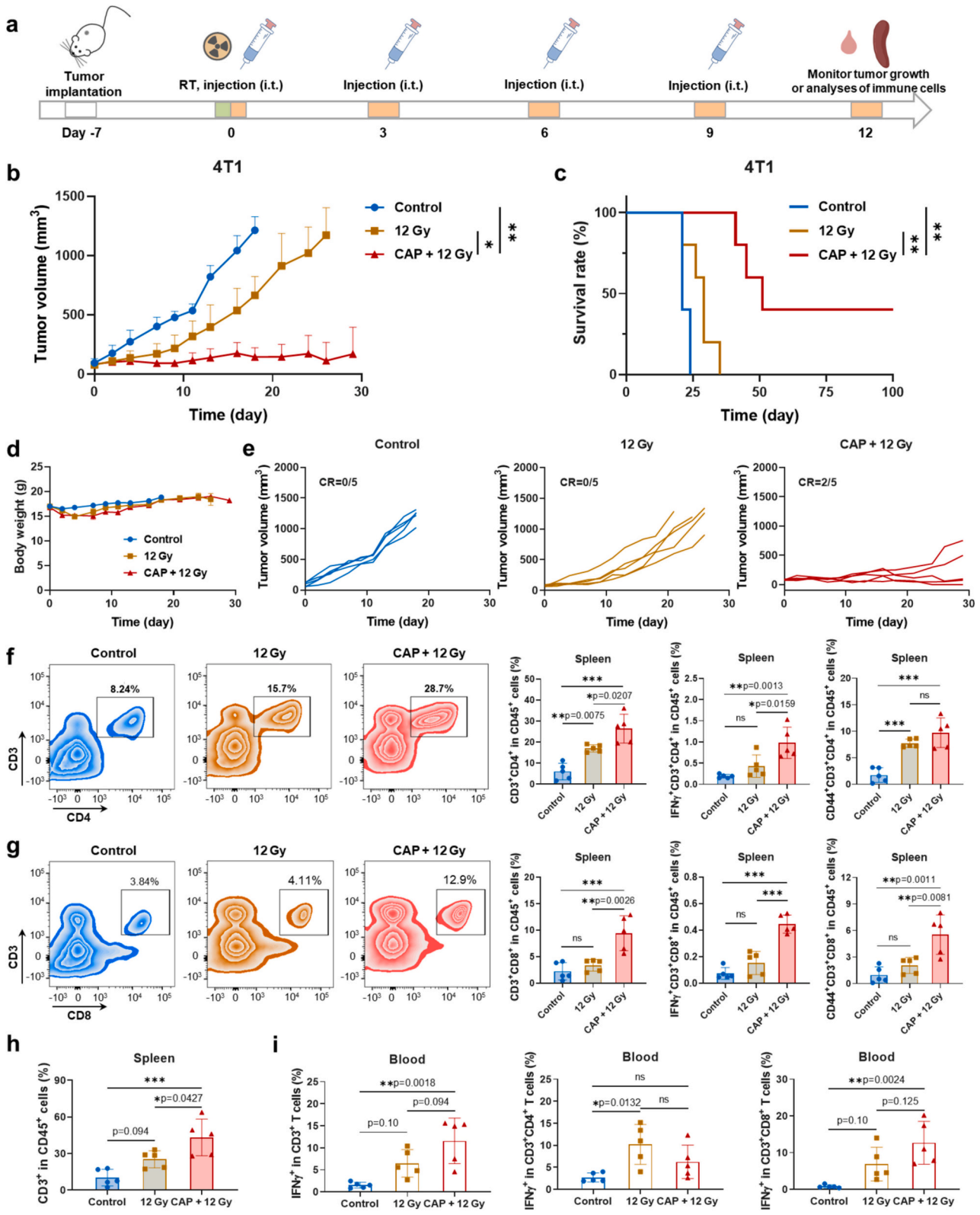

Fig. 3. CAP improves the anti-tumor immunity generated by 12 Gy RT in murine 4T1 breast tumor-bearing mice. (a) Schematic illustration of the anti-tumor studies and the analyses of the immune response in spleens and blood on 4T1 breast tumor-bearing mice. (b) Average tumor growth curves, (c) survival rate and (d) average body weight of mice after the indicated treatments ($n = 5$). (e) Individual tumor growth curves in (b). (f) Representative flow cytometry analysis of $CD3^+CD4^+$ T cells and percentages of $CD3^+CD4^+$ T cells, $IFN\gamma^+$ CD4 T cells and $CD44^+$ CD4 T cells among $CD45^+$ splenocytes after the indicated treatments were performed on 4T1 breast tumor-bearing mice. (g) Representative flow cytometry analysis of $CD3^+CD8^+$ T cells and percentages of $CD3^+CD8^+$ T cells, $IFN\gamma^+$ CD8 T cells and $CD44^+$ CD8 T cells among $CD45^+$ splenocytes after the indicated treatments were performed on 4T1 breast tumor-bearing mice. (h) Percentages of $CD3^+$ T cells among $CD45^+$ splenocytes after the indicated treatments were performed on 4T1 breast tumor-bearing mice. (i) Percentages of $IFN\gamma^+$ cells among $CD3^+$, $CD3^+CD4^+$ and $CD3^+CD8^+$ T cells in the blood after the indicated treatments were performed on 4T1 breast tumor-bearing mice (n = 5). CR: Complete response. Statistical significance was calculated via one-way ANOVA test in b and f-i, and log-rank test in c. The data are presented as mean ± SD. $^*p < 0.05$, $^{**}p < 0.01$, $^{***}p < 0.001$.

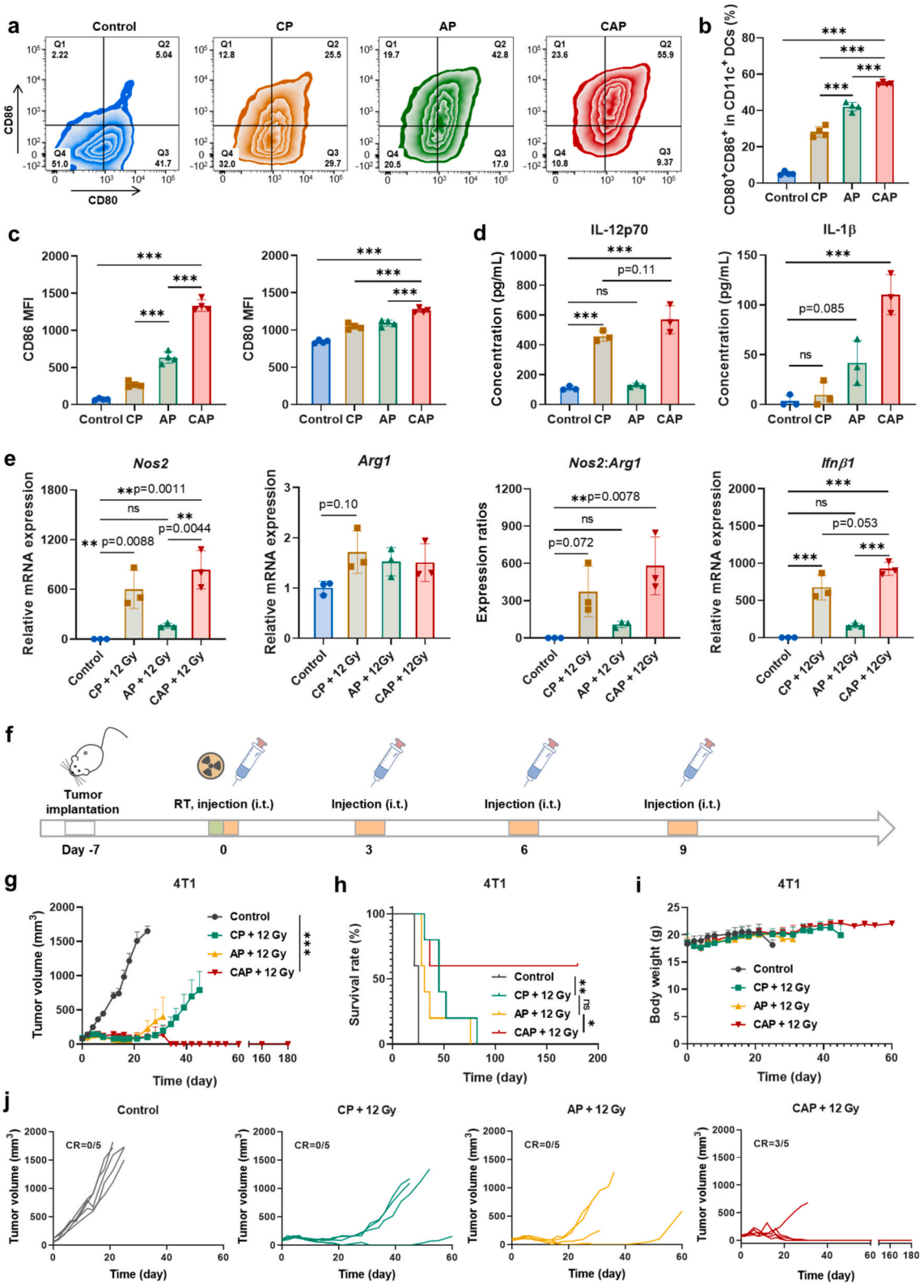

Fig. 4. Dual immune activation nano-agonist CAP is more effective than its single immune activation nano-agonist counterparts on eliciting a robust anti-tumor immune response. (a) Representative flow cytometry analysis of the activation of BMDCs after treatment with CP, AP or CAP. (b) Percentages of $CD80^{+}CD86^{+}$ cells among BMDCs after treatment with CP, AP or CAP. (c) MFI indicated CD86 (left) and CD80 (right) expression on BMDCs after treatment with CP, AP or CAP ($n = 4$). (d) Levels of IL-12p70 and IL-1β in the supernatant of BMDCs after treatment with CP, AP or CAP ($n = 3$). (e) Expression of *Nos2*, *Arg1*, *Ifnβ1* and expression ratios of *Nos2*:*Arg1* in RAW264.7 macrophages after treatment with CP, AP or CAP (n = 3). (f) Schematic illustration of the anti-tumor studies on 4T1 breast tumor-bearing mice. (g) Average tumor growth curves, (h) survival rates and (i) average body weights of mice after the indicated treatments ($n = 5$). (j) Individual tumor growth curves in (g). CR: Complete response. Statistical significance was calculated via one-way ANOVA test in b-e and g, and the log-rank test in h. The data are presented as mean ± SD. $^{*}p < 0.05$, $^{**}p < 0.01$, $^{***}p < 0.001$.

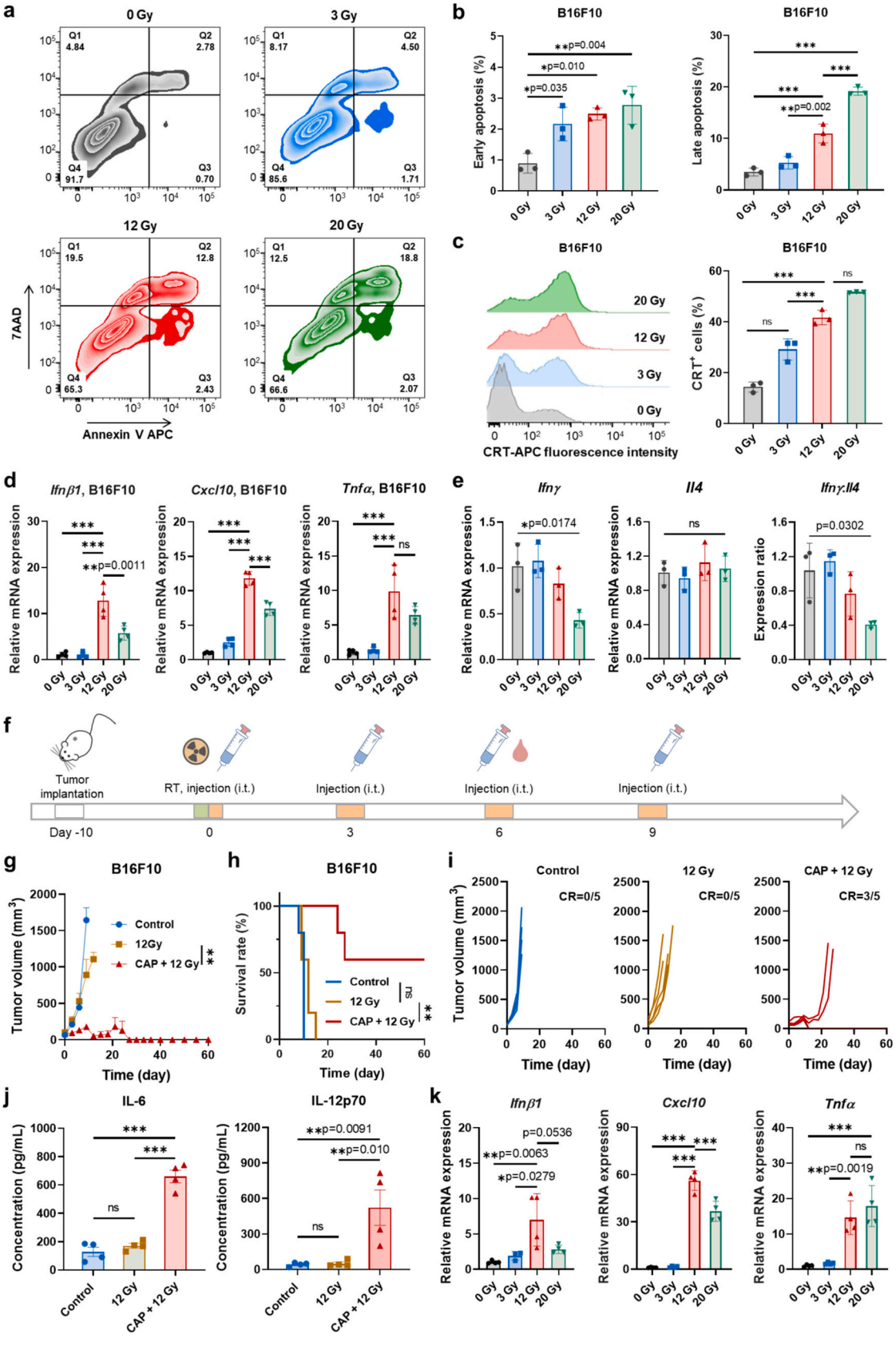

(caption on next page)

Fig. 5. 12 Gy irradiation effectively optimizes the immunogenicity of multiple tumor cells and CAP significantly potentiates the in situ vaccination effects of 12 Gy RT. (a) Representative flow cytometry analysis of the apoptosis of B16F10 cells and (b) percentages of early apoptosis and late apoptosis among B16F10 cells at 24 h after irradiation at different doses ($n = 3$). (c) Histogram graphs of CRT expression in B16F10 cells and percentages of CRT^+ B16F10 cells at 24 h after irradiation at different doses (n = 3). (d) Relative expression of *Ifnβ1*, *Cxcl10* and *Tnfα* in B16F10 cells at 48 h after irradiation at different doses ($n = 4$). (e) Relative expression of *Ifnγ* and *Il4* and expression ratios of *Ifnγ:Il4* in splenocytes at 24 h after co-culture with the supernatants of irradiated B16F10 cells (n = 3). The treatment was performed per Fig. 2e. (f) Schematic illustration of the anti-tumor studies on B16F10 melanoma-bearing mice. (g) Average tumor growth curves and (h) survival rates of mice after the indicated treatments ($n = 5$). (i) Individual tumor growth curves in (g). (j) Levels of IL-6 and IL-12p70 in the serum of B16F10 melanoma-bearing mice after the indicated treatments (n = 4). (k) Relative expression of *Ifnβ1*, *Cxcl10* and *Tnfα* in HeLa cells at 48 h after irradiation at different doses (n = 4). CR: Complete response. Statistical significance was calculated via one-way ANOVA test in b-e, g and j-k, and the log-rank test in h. The data are presented as mean ± SD. $^*p < 0.05$, $^{**}p < 0.01$, $^{***}p < 0.001$.

enhanced the immunogenicity of B16F10 melanoma cells. As shown in Fig. 5a-5c and S11-S12, we found that both 12 Gy and 20 Gy irradiation induced immunogenic late apoptosis/secondary necrosis and ICD in B16F10 melanoma cells. Furthermore, we studied the effects of RT on priming immune cytokines in B16F10 melanoma cells and found that 12 Gy irradiation had greater effects on stimulating the production of immune cytokines, including *Ifnβ1*, *Cxcl10* and *Tnfα*, than either 3 Gy or 20 Gy irradiation (Fig. 5d). However, similar to our observation in 4T1 cells, we noted that the supernatants from irradiated B16F10 melanoma cells were immunosuppressive in modulating the anti-tumor effects of T cells, leading to decreased *Ifnγ:Il4* expression ratios, and this effect could be reversed by CAP treatment (Fig. 5e and S13). These in vitro results strongly validated the effects of 12 Gy RT in optimally enhancing the immunogenicity of B16F10 melanoma cells and its adverse regulatory effects on T cell polarization, which necessitated the inclusion of the dual immune activation nano-agonist CAP to overcome the immunosuppressive obstacles and implied the optimized anti-tumor immune response induced by the combination of 12 Gy RT and CAP. To verify this, we established subcutaneous xenograft B16F10 melanoma-bearing mice, irradiated the tumor sites at 12 Gy and intratumorally injected CAP into the irradiated tumors (Fig. 5f). We found that 12 Gy RT treated mice exhibited comparable tumor growth and mouse survival to those of untreated control mice, while CAP significantly augmented the tumor eradication by 12 Gy RT, resulting in prolonged mouse survival and three out of five mice being disease-free after treatment (Fig. 5g-5i). Analysis of the serum collected from mice after treatment revealed that CAP +12 Gy RT treated mice exhibited higher levels of IL-6 and IL-12p70 than both untreated control mice and 12 Gy irradiated mice, suggesting a potent immune response (Fig. 5j). These results implied the generalizability of the in situ cancer vaccine induced by CAP +12 Gy RT in multiple murine tumor models. Furthermore, to determine whether 12 Gy RT is optimal for modulating the immunogenicity of human cancer cells, we employed HeLa cells, a type of human cervical cancer cell line, to evaluate the expression of immune cytokines after irradiation at different doses. As shown in Fig. 5k, although 12 Gy and 20 Gy irradiation were more effective than 3 Gy in generating the expression of *Tnfα* in HeLa cells, 12 Gy irradiation had a significantly greater effect on the priming of *Ifnβ1* and *Cxcl10* than both 3 Gy and 20 Gy irradiation. These findings suggest the optimized effects of 12 Gy RT in modulating the immunogenicity of human cancer cells and indicate the potential of the CAP +12 Gy RT treatment regimen in generating robust in situ vaccination effects in human cancer settings.

3.5. Dual immune activation nano-agonist plus radiotherapy induces a systemic anti-tumor immune response and immune memory effects

Metastatic and circulating tumor cells pose significant challenges leading to poor prognosis in clinical cancer treatment [48,49]. In situ cancer vaccines that are capable of eliciting systemic anti-tumor immune responses offer promising potential for eradicating not only targeted tumors but also distant tumors located elsewhere in the body that are not directly treated with in situ vaccine regimens. To assess whether the in situ cancer vaccine primed by CAP +12 Gy RT could generate systemic anti-tumor immunity, we treated 4T1 breast tumor-bearing mice with the CAP +12 Gy RT treatment regimen and re-challenged these mice contralaterally on day 28 since the initiation of treatment (Fig. 6a).Consistent with the previously observed results, CAP +12 Gy RT treatment significantly suppressed the growth of pre-inoculated 4T1 tumors, resulting in six out of eight mice being tumor-free (Fig. 6b-6c). Analyses of circulating T cells revealed that the untreated control mice exhibited obvious lymphopenia with a decrease in the abundance of circulating T lymphocytes, possibly associated with the 4T1 breast tumor burden at approximately 600–900 mm^3 (Fig. S14). Intriguingly, lymphopenia in 4T1 tumor-bearing mice was reversed by CAP +12 Gy RT treatment, with the proportions of T lymphocytes, including both CD4 and CD8 T lymphocytes, returning to normal levels in the CAP +12 Gy RT treated mice (Fig. 6f). Moreover, the CAP +12 Gy RT treatment regimen demonstrated potent abscopal effects, significantly slowing the growth of contralateral re-challenged 4T1 breast tumors (Fig. 6d-6e). To explore the immune populations associated with systemic anti-tumor immune response, we analyzed contralateral re-challenged tumors and spleens from the mice (Fig. S15-S16). As shown in Fig. 6g, we observed a trend toward increased percentages of both $CD8^+CD3^+$ T cells and $CD3^-NK1.1^+$ cells among $CD45^+$ cells in the re-challenged tumors following CAP +12 Gy RT treatment, while the abundance of $CD4^+CD3^+$ T cells remained relatively unchanged. Examination of memory immune cells in spleens revealed elevated levels of both $CD44^+CD62L^-$ effector memory T cells (Tem) and $CD44^+CD62L^+$ central memory T cells (Tcm) among $CD8^+CD3^+$ T cells with CAP +12 Gy RT treatment, along with a tendency for increased percentages of $CD44^+CD62L^-$ Tem among $CD4^+CD3^+$ T cells (Fig. 6h-6i). These findings highlight the critical roles of CD8 T cells in systemic anti-tumor immunity and immune memory effects induced by CAP +12 Gy RT treatment.

Rapid postoperative tumor recurrence and cancer metastasis are among the major threats leading to cancer-related mortality [50]. Therefore, a potent tumor-specific immune response capable of preventing tumor relapse and metastasis holds promise for effective cancer management. To explore this, we established a postoperative tumor model and examined the effects of CAP +12 Gy RT treatment on managing recurrent and metastatic tumors (Fig. 7a). The in vivo imaging system (IVIS) images are shown in Fig. 7b, and the data are shown in Fig. 7d-7f. Although 12 Gy RT treatment attenuated the growth of recurrent tumors, it was poor in complete tumor eradication. In contrast, CAP +12 Gy RT treatment effectively eliminated relapsed tumors post-operation, resulting in seven out of nine mice being disease-free after treatment. Notably, local CAP +12 Gy RT treatment significantly prevented the lung metastasis of tumors (Fig. 7c). These findings suggested the remarkable performance of CAP +12 Gy RT treatment in not only eliminating local tumors but also combating circulating tumor cells to prevent tumor metastasis. Furthermore, to examine whether local CAP +12 Gy RT treatment can generate an "abscopal effect" to inhibit the growth of pre-existing distant untreated tumors, we generated two 4T1 tumors-bearing mice with one implanted on the right flank and the other implanted on the left flank five days later to simulate a smaller metastatic tumor (Fig. 7g). CAP +12 Gy RT treatment was performed on the right tumor only. Consistent with prior reports, 12 Gy RT alone slowed the growth of treated right flank tumors but had poor abscopal effects, and the growth of distant untreated tumors in 12 Gy-irradiated mice was similar to that in untreated control mice (Fig. 7h-7i and S17) [43].

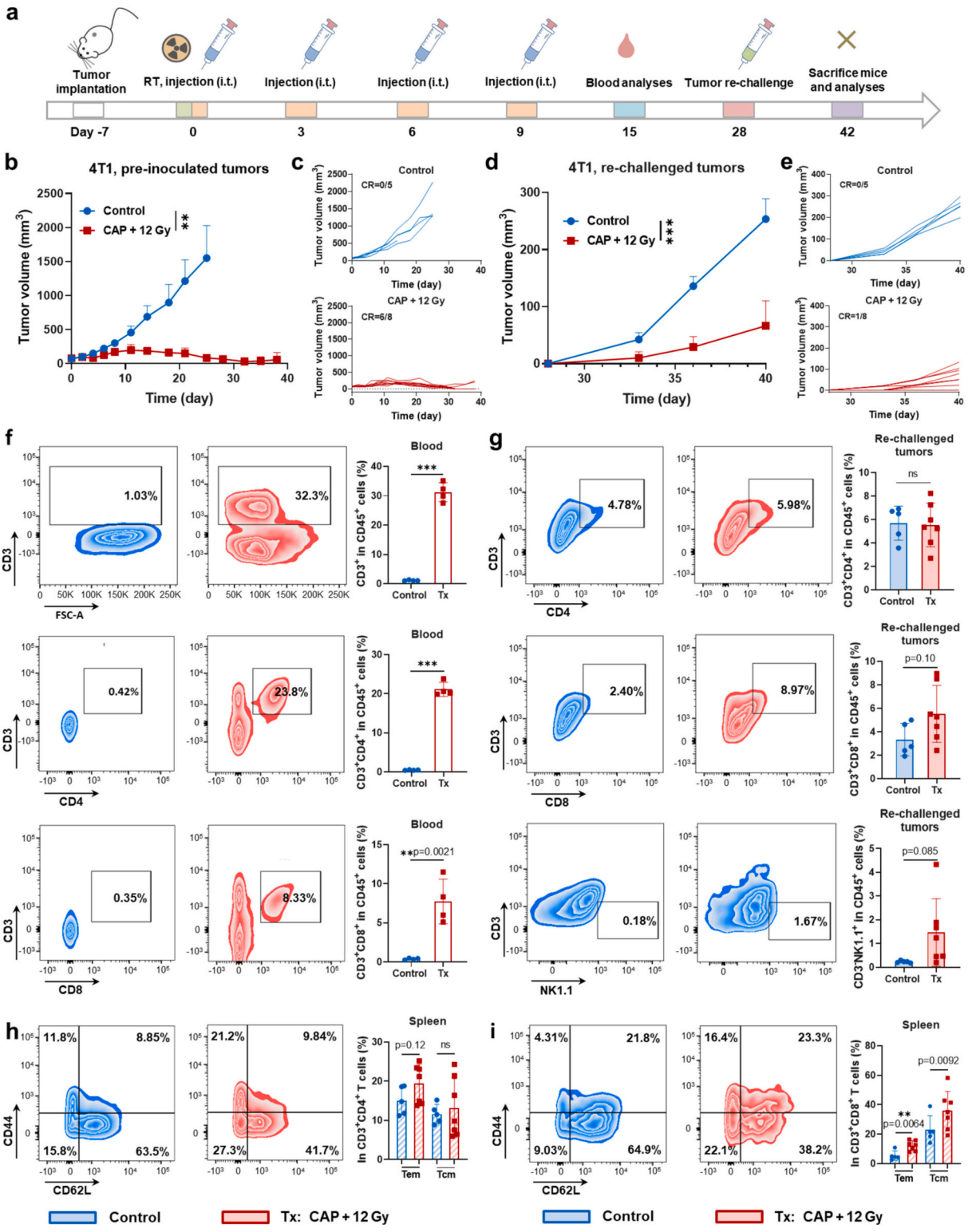

Fig. 6. CAP +12 Gy RT treatment elicited a systemic anti-tumor immune response with memory effects. (a) Schematic illustration of the studies on 4T1 breast tumor-bearing mice. (b) Average tumor growth curves of pre-inoculated 4T1 breast tumors after the indicated treatments (Control: $n = 5$; CAP +12 Gy RT: $n = 8$). (c) Individual tumor growth curves in (b). (d) Average tumor growth curves of re-challenged 4T1 breast tumors (Control: n = 5; CAP +12 Gy RT: n = 8). (e) Individual tumor growth curves in (d). (f) Representative flow cytometry analysis of $CD3^+$ T cells, $CD4^+CD3^+$ T cells and $CD8^+CD3^+$ T cells among $CD45^+$ cells in blood and their quantitative percentages after the indicated treatments ($n = 4$). (g) Representative flow cytometry analysis of $CD4^+CD3^+$ T cells, $CD8^+CD3^+$ T cells and $CD3^-NK1.1^+$ NK cells among $CD45^+$ cells in the re-challenged 4T1 breast tumors and their quantitative percentages after the indicated treatments (Control: n = 5; Tx: $n = 7$). (h) Representative flow cytometry analysis of Tem ($CD44^+CD62L^-$) and Tcm ($CD44^+CD62L^+$) among $CD4^+CD3^+$ T cells in spleens and their quantitative percentages after the indicated treatments (Control: n = 5; Tx: n = 7). (i) Representative flow cytometry analysis of Tem ($CD44^+CD62L^-$) and Tcm ($CD44^+CD62L^+$) among $CD8^+CD3^+$ T cells in spleens and their quantitative percentages after the indicated treatments (Control: n = 5; Tx: n = 7). The mice free from re-challenged 4T1 breast tumors were not used for the analyses of tumors or spleens. CR: Complete response. Statistical significance was calculated via unpaired *t*-test in b, d and f-i. The data are presented as mean ± SD. $^*p < 0.05$, $^{**}p < 0.01$, $^{***}p < 0.001$.

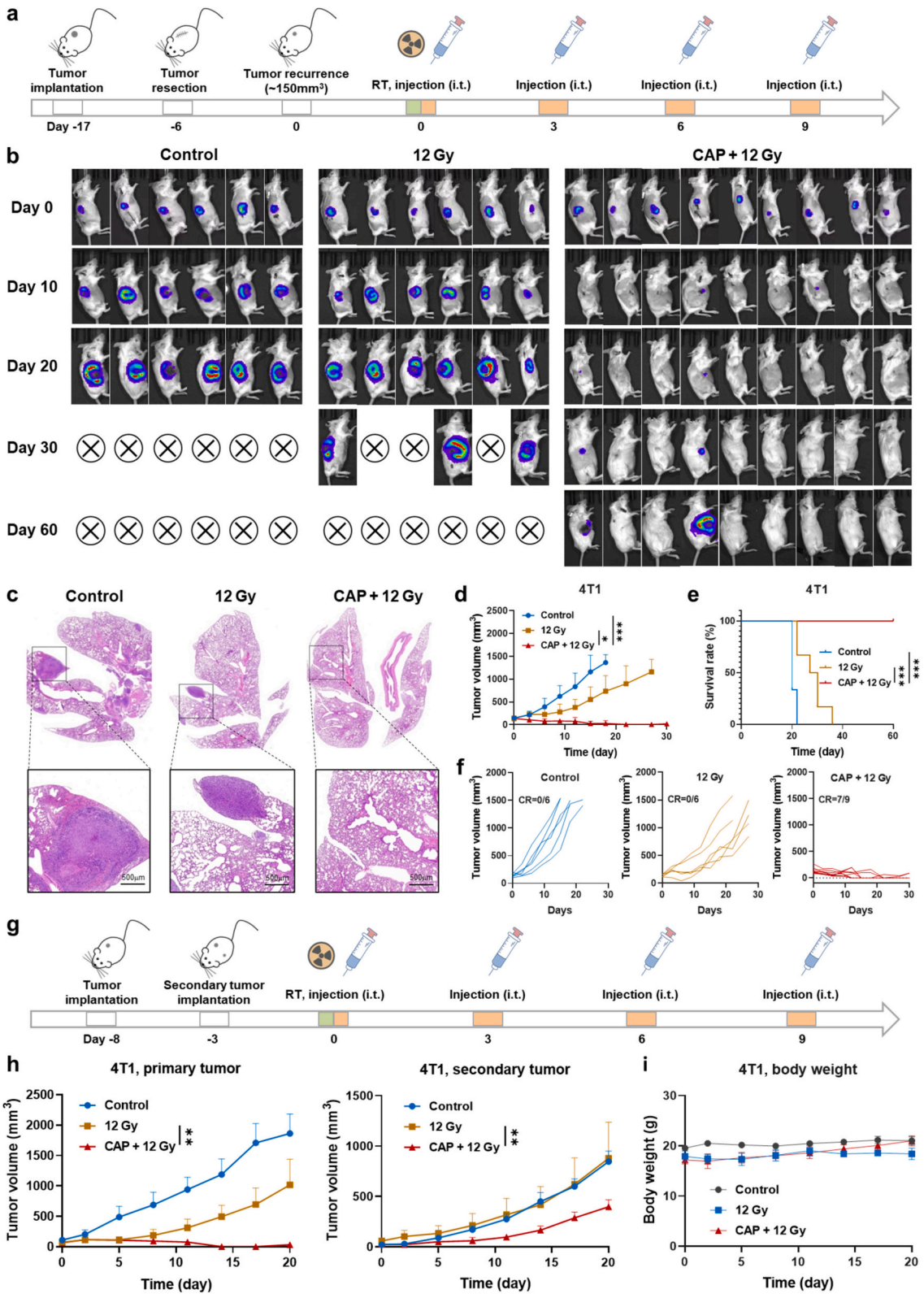

Fig. 7. CAP plus 12 Gy RT treatment effectively eradicated postoperative recurrent tumors, prevented tumor metastasis and suppressed the growth of distant tumors that were not directly treated. (a) Schematic illustration of the studies on postoperative 4T1-Luc breast tumor-bearing mice. (b) Bioluminescence images of 4T1-Luc tumors on days 0, 10, 20, 30 and 60 since the initiation of treatment. (c) Images of H&E stained sections of lungs at day 30 since the initiation of treatment. (d) Average tumor growth curves of relapsed 4T1-Luc breast tumors and (e) survival rates of mice after the indicated treatments (Control and 12 Gy: $n = 6$; CAP +12 Gy RT: $n = 9$). (f) Individual tumor growth curves in (d). (g) Schematic illustration of the studies on 4T1 two tumors-bearing mice. (h) Average tumor growth curves of primary tumors and distant tumors after the indicated treatments. (i) Average body weight of mice after the indicated treatments (Control and 12 Gy: $n = 5$; CAP +12 Gy RT: n = 6). CR: Complete response. Statistical significance was calculated via one-way ANOVA test in d and h, and the log-rank test in e. The data are presented as mean ± SD. *$p < 0.05$, **$p < 0.01$, ***$p < 0.001$.

Importantly, we revealed that CAP +12Gy RT treatment not only eliminated the target tumors with four out of six mice exhibiting complete responses, but also attenuated the advancement of distant untreated tumors. No significant changes in animal weight were observed in the treatment group in this study (Fig. 7h-7i and S17).

4. Discussion

The rising demands to bypass the time-intensive processes of tumor antigen identification and synthesis urged the development of in situ vaccination strategies. Focal RT has shown promise in priming in situ vaccination effects, though so far only modest and short-lived immune responses are achieved. In this study, we developed a robust in situ cancer vaccine by optimizing radiation dose and employing a dual-immune activation nano-agonist (CAP) that co-targets STING-TLR9 pathways to eradicate solid tumors. Collectively, our results show 12Gy RT was optimal to increase the immunogenicity of tumor cells, while CAP effectively reversed the immunosuppression induced by 12Gy RT and enhanced immune activation post-RT, thereby positively regulating the tumor microenvironment. We demonstrated that this in situ vaccination strategy not only extended the local therapeutic effects of RT to distant untreated tumors through a systemic anti-tumor immune response but also significantly reduced the incidence of recurrent tumors and lung metastases in a postoperative murine tumor model.

Currently, comprehensive comparisons of the immunomodulatory potential of radiation at different doses on both tumor cell immunogenicity and immune cell functions are lacking, despite their critical importance in constructing a robust in situ cancer vaccine. To develop a clinically meaningful in situ cancer vaccine using RT, we aimed to identify an optimal radiation dose from four commonly employed in clinical settings based on their immunomodulatory effects. In vitro studies demonstrated that radiation induced apoptosis and ICD of 4T1 breast tumor cells in a dose-dependent manner that 12Gy and 20Gy irradiation show more pronounced effects (Fig. 1). Previous studies have suggested that ~12Gy radiation may be optimal for stimulating the cGAS-STING pathway, resulting in an IFN-I immune response in tumor cells[12,51]. In this study, radiation at 12Gy was revealed to be effective in increasing the expression of not only *Ifnβ* but also *Cxcl10* and *Tnfα* in tumor cells (Fig. 1), and these cytokines are essential for T cell recruitment and APC maturation during in situ vaccination. These findings were corroborated in murine aggressive B16F10 melanoma cells and human cervical cancer HeLa cells (Fig. 5). However, despite these promising results, in vitro evaluations also revealed that radiation at the tested doses promoted the polarization of macrophages toward the anti-inflammatory M2 phenotype, and radiation-primed tumor cell metabolites skewed T cells toward the Th2/Tc2 phenotype (Fig. 1 and Fig. 5). These results suggest the great potential of 12Gy RT in priming a robust in situ cancer vaccine but also highlight the necessity of specific immunomodulators to address the immunosuppressive effects induced by RT to achieve significant anti-tumor effects.

A CAST strategy was developed based on a dual immune activation nano-agonist CAP that *co*-encapsulated the TLR9 agonist CpG and the cGAS-STING agonist ADU-S100 into a polymersome to overcome the immunosuppressive obstacles generated by 12Gy RT. CAP was demonstrated to effectively antagonize the detrimental polarization of BMDMs and T cells induced by radiation in vitro (Fig. 2), indicating its potential to create a favorable immunostimulatory tumor microenvironment. In vivo studies further revealed that intratumoral administration of CAP significantly enhanced the anti-tumor immune response induced by 12Gy RT. In both the murine 4T1 breast tumor model and murine B16F10 melanoma model, the CAP +12Gy RT treatment resulted in greater tumor eradication and prolonged mouse survival compared to treatment with 12Gy RT or CAP alone (Figs. 3, 5 and S6). Moreover, additional investigations demonstrated that local CAP +12Gy RT treatment primed tumor-specific immune memory effects and robust systemic anti-tumor immunity, even in tumors not directly treated by 12Gy RT or CAP injection, thereby suppressing the growth of distant untreated tumors (Figs. 6 and 7). Notably, the CAP +12Gy treatment regimen showed negligible systemic toxicity (Fig. S9).

Several limitations remain in this study. Firstly, our focus was on radiation with a single fraction. To gain a more comprehensive understanding of the immunomodulation effects of radiation across broader fractionated regimens, further evaluation is warranted. Secondly, it will be valuable to optimize the timing and dosing of CAP injection to further improve the anti-tumor efficacy while minimizing detrimental side effects. Although intratumoral injection has been approved by the U.S. Food and Drug Administration (FDA) for multiple therapeutics, it would be important to modify the formulation and manufacturing of CAP in future studies to achieve high accumulation in tumor tissues after intravenous administration. This would address the treatment needs of tumors inaccessible for intratumoral administration or located in deep tissues. Since it has been reported that radiation can prime tumors to drive the accumulation of nanotherapeutics [52,53], it would be a promising opportunity to achieve a robust in situ cancer vaccine by RT and intravenously administrated nano-agonists. Moreover, although previous studies have suggested that the dose-dependent induction of IFN-I responses in tumor cells may be related to the DNA exonuclease Trex1 [12], future investigations need to focus on the molecular signaling pathways through which radiotherapy at different dosages modulates responses in immune cells, which could provide valuable insights into potential therapeutic targets for mitigating radiotherapy-induced immunosuppression and enhancing the efficacy of in situ cancer vaccines.

Despite these limitations, this work presents a straightforward in situ cancer vaccination strategy by selecting a dose of RT with optimal immunostimulatory effects and fabricating nano-agonists CAP to alleviate the detrimental immunosuppression caused by RT. The excellent biocompatibility of CAP +12Gy RT treatment and its effective tumor eradication across different tumor models highlight its potential for translation into clinical cancer therapy.

5. Conclusion

In situ vaccines offer a straightforward approach to generate tumor-specific immune response for tumor eradication. However, current in situ vaccines generally produce modest and short-lived immune responses, limiting their clinical translation. In this study, we aimed to construct robust in situ cancer vaccines based on clinical RT. We investigated the immunomodulatory effects of radiation at different dosages and found that 12Gy RT exhibited the strongest immunostimulatory effect on tumor cells among the tested dosages, but it also had a suppressive effect on the immunoregulation of macrophages and T cells. To construct a robust in situ cancer vaccine, we selected 12Gy RT and developed a dual immune activation nano-agonist CAP to antagonize its immunosuppressive effects. In different murine tumor models, the CAP +12Gy RT in situ vaccination strategy demonstrated robust anti-tumor immune responses with systemic and memory effects, highlighting its potential for clinical translation.

CRediT authorship contribution statement

Yu Sun: Writing – original draft, Methodology, Investigation, Formal analysis, Data curation, Conceptualization. **Liang Liu:** Methodology, Investigation, Funding acquisition, Formal analysis. **Huilan He:** Methodology, Investigation, Formal analysis. **Guanhong Cui:** Methodology, Investigation, Formal analysis. **Yun Zheng:** Methodology, Investigation, Formal analysis. **Chunlian Ye:** Methodology, Investigation, Formal analysis. **Liping Qu:** Methodology, Investigation, Formal analysis. **Yinping Sun:** Methodology, Investigation, Formal analysis. **Jinlong Ji:** Methodology, Investigation, Formal analysis. **Twan Lammers:** Writing – original draft, Conceptualization. **Ying Zhang:** Writing – review & editing, Writing – original draft, Funding acquisition, Data curation,

Conceptualization. **Zhiyuan Zhong:** Writing – review & editing, Funding acquisition, Conceptualization.

Declaration of competing interest

The authors declare no competing financial interest.

Acknowledgments

This work was financially supported by the National Natural Science Foundation of China (52303199, 52233007), the Natural Science Foundation of Jiangsu Province (BK20210944), and the Natural Science Foundation of the Jiangsu Higher Education Institutions of China (23KJB350006).

Appendix A. Supplementary data

Supplementary data to this article can be found online at https://doi.org/10.1016/j.jconrel.2024.12.079.

Data availability

The data that support the findings of this study are available from the corresponding author upon reasonable request.

References

[1] H. Lei, Z. Pei, C. Jiang, L. Cheng, Recent progress of metal-based nanomaterials with anti-tumor biological effects for enhanced cancer therapy, Exploration 3 (5) (2023) 20220001.
[2] G. Yang, J. Ding, X. Chen, Bioactive poly(amino acid)s for multi-modal cancer therapy, WIREs Nanomed. Nanobiotechnol. 16 (4) (2024) e1985.
[3] Y. Li, Y. Wu, Z. Fang, Y. Zhang, H. Ding, L. Ren, L. Zhang, Q. Gong, Z. Gu, K. Luo, Dendritic nanomedicine with boronate bonds for augmented chemo-immunotherapy via synergistic modulation of tumor immune microenvironment, Adv. Mater. 36 (2) (2024) 2307263.
[4] W. Xu, Y. Su, Y. Ma, Q. Wei, J. Yang, X. Zhuang, J. Ding, X. Chen, Immunologically effective poly(D-lactic acid) nanoparticle enhances anticancer immune response, Sci. China Chem. 66 (4) (2023) 1150–1160.
[5] M.J. Lin, J. Svensson-Arvelund, G.S. Lubitz, A. Marabelle, I. Melero, B.D. Brown, J. D. Brody, Cancer vaccines: the next immunotherapy frontier, Nat. Can. 3 (8) (2022) 911–926.
[6] C. Feng, P. Tan, G. Nie, M. Zhu, Biomimetic and bioinspired nano-platforms for cancer vaccine development, Exploration 3 (3) (2023) 20210263.
[7] E. Blass, P.A. Ott, Advances in the development of personalized neoantigen-based therapeutic cancer vaccines, Nat. Rev. Clin. Oncol. 18 (4) (2021) 215–229.
[8] Ö. Türeci, M. Löwer, B. Schrörs, M. Lang, A. Tadmor, U. Sahin, Challenges towards the realization of individualized cancer vaccines, Nat. Biomed. Eng. 2 (8) (2018) 566–569.
[9] M. Saxena, S.H. van der Burg, C.J.M. Melief, N. Bhardwaj, Therapeutic cancer vaccines, Nat. Rev. Cancer 21 (6) (2021) 360–378.
[10] J. Chen, M. Qiu, Z. Ye, T. Nyalile, Y. Li, Z. Glass, X. Zhao, L. Yang, J. Chen, Q. Xu, In situ cancer vaccination using lipidoid nanoparticles, Sci. Adv. 7 (2021) eabf1244.
[11] N. Gong, M.-G. Alameh, R. El-Mayta, L. Xue, D. Weissman, M.J. Mitchell, Enhancing in situ cancer vaccines using delivery technologies, Nat. Rev. Drug Discov. 23 (2024) 607–625.
[12] C. Vanpouille-Box, A. Alard, M.J. Aryankalayil, Y. Sarfraz, J.M. Diamond, R. J. Schneider, G. Inghirami, C.N. Coleman, S.C. Formenti, S. Demaria, DNA exonuclease Trex1 regulates radiotherapy-induced tumour immunogenicity, Nat. Commun. 8 (1) (2017) 15618.
[13] Z. Huang, R. Gu, S. Huang, Q. Chen, J. Yan, X. Cui, H. Jiang, D. Yao, C. Shen, J. Su, T. Liu, J. Wu, Z. Luo, Y. Hu, A. Yuan, Chiral coordination polymer nanowires boost radiation-induced in situ tumor vaccination, Nat. Commun. 15 (1) (2024) 3902.
[14] R.B. Patel, R. Hernandez, P. Carlson, J. Grudzinski, A.M. Bates, J.C. Jagodinsky, A. Erbe, I.R. Marsh, I. Arthur, E. Aluicio-Sarduy, R.N. Sriramaneni, W.J. Jin, C. Massey, A.L. Rakhmilevich, D. Vail, J.W. Engle, T. Le, K. Kim, B. Bednarz, P. M. Sondel, J. Weichert, Z.S. Morris, Low-dose targeted radionuclide therapy renders immunologically cold tumors responsive to immune checkpoint blockade, Sci. Transl. Med. 13 (2021) eabb3631.
[15] S.C. Formenti, N.-P. Rudqvist, E. Golden, B. Cooper, E. Wennerberg, C. Lhuillier, C. Vanpouille-Box, K. Friedman, L. Ferrari de Andrade, K.W. Wucherpfennig, A. Heguy, N. Imai, S. Gnjatic, R.O. Emerson, X.K. Zhou, T. Zhang, A. Chachoua, S. Demaria, Radiotherapy induces responses of lung cancer to CTLA-4 blockade, Nat. Med. 24 (12) (2018) 1845–1851.
[16] W.S.M.E. Theelen, H.M.U. Peulen, F. Lalezari, V. van der Noort, J.F. de Vries, J.G.J. V. Aerts, D.W. Dumoulin, I. Bahce, A.-L.N. Niemeijer, A.J. de Langen, K. Monkhorst, P. Baas, Effect of pembrolizumab after stereotactic body radiotherapy vs pembrolizumab alone on tumor response in patients with advanced non–small cell lung cancer, JAMA Oncol. 5 (9) (2019) 1276–1282.
[17] R.B. Patel, M. Ye, P.M. Carlson, A. Jaquish, L. Zangl, B. Ma, Y. Wang, I. Arthur, R. Xie, R.J. Brown, X. Wang, R. Sriramaneni, K. Kim, S. Gong, Z.S. Morris, Development of an in situ cancer vaccine via combinational radiation and bacterial-membrane-coated nanoparticles, Adv. Mater. 31 (43) (2019) 1902626.
[18] P. Xu, J. Ma, Y. Zhou, Y. Gu, X. Cheng, Y. Wang, Y. Wang, M. Gao, Radiotherapy-triggered in situ tumor vaccination boosts checkpoint blockaded immune response via antigen-capturing nanoadjuvants, ACS Nano 18 (1) (2023) 1022–1040.
[19] K. Ni, G. Lan, N. Guo, A. Culbert, T. Luo, T. Wu, R.R. Weichselbaum, W. Lin, Nanoscale metal-organic frameworks for x-ray activated in situ cancer vaccination, Sci. Adv. 6 (2020) eabb5223.
[20] J.C. Jagodinsky, A.M. Bates, P.A. Clark, R.N. Sriramaneni, T.C. Havighurst, I. Chakravarty, E.J. Nystuen, K. Kim, P.M. Sondel, W.J. Jin, Z.S. Morris, Local TLR4 stimulation augments in situ vaccination induced via local radiation and anti-CTLA-4 checkpoint blockade through induction of CD8 T-cell independent Th1 polarization, J. Immunother. Cancer 10 (10) (2022) e005103.
[21] R.R. Weichselbaum, H. Liang, L. Deng, Y.-X. Fu, Radiotherapy and immunotherapy: a beneficial liaison? Nat. Rev. Clin. Oncol. 14 (6) (2017) 365–379.
[22] U.M. Cytlak, D.P. Dyer, J. Honeychurch, K.J. Williams, M.A. Travis, T.M. Illidge, Immunomodulation by radiotherapy in tumour control and normal tissue toxicity, Nat. Rev. Immunol. 22 (2) (2021) 124–138.
[23] Y. Zhang, R.N. Sriramaneni, P.A. Clark, J.C. Jagodinsky, M. Ye, W. Jin, Y. Wang, A. Bates, C.P. Kerr, T. Le, R. Allawi, X. Wang, R. Xie, T.C. Havighurst, I. Chakravarty, A.L. Rakhmilevich, K.A. O'Leary, L.A. Schuler, P.M. Sondel, K. Kim, S. Gong, Z.S. Morris, Multifunctional nanoparticle potentiates the in situ vaccination effect of radiation therapy and enhances response to immune checkpoint blockade, Nat. Commun. 13 (1) (2022) 4948.
[24] J. Baba, S. Watanabe, Y. Saida, T. Tanaka, T. Miyabayashi, J. Koshio, K. Ichikawa, K. Nozaki, T. Koya, K. Deguchi, C. Tan, S. Miura, H. Tanaka, J. Tanaka, H. Kagamu, H. Yoshizawa, K. Nakata, I. Narita, Depletion of radio-resistant regulatory T cells enhances antitumor immunity during recovery from lymphopenia, Blood 120 (12) (2012) 2417–2427.
[25] H.E. Barker, J.T.E. Paget, A.A. Khan, K.J. Harrington, The tumour microenvironment after radiotherapy: mechanisms of resistance and recurrence, Nat. Rev. Cancer 15 (7) (2015) 409–425.
[26] X. Guan, L. Sun, Y. Shen, F. Jin, X. Bo, C. Zhu, X. Han, X. Li, Y. Chen, H. Xu, W. Yue, Nanoparticle-enhanced radiotherapy synergizes with PD-L1 blockade to limit post-surgical cancer recurrence and metastasis, Nat. Commun. 13 (1) (2022) 2834.
[27] C. Wang, Z. Dong, Y. Hao, Y. Zhu, J. Ni, Q. Li, B. Liu, Y. Han, Z. Yang, J. Wan, K. Yang, Z. Liu, L. Feng, Coordination polymer-coated CaCO3 reinforces radiotherapy by reprogramming the immunosuppressive metabolic microenvironment, Adv. Mater. 34 (3) (2022) 2106520.
[28] Q. Chen, J. Chen, Q. Zhang, P. Yang, R. Gu, H. Ren, Y. Dai, S. Huang, J. Wu, X. Wu, Y. Hu, A. Yuan, Combining high-Z sensitized radiotherapy with CD73 blockade to boost tumor immunotherapy, ACS Nano 17 (13) (2023) 12087–12100.
[29] P. Yao, Y. Zhang, H. Meng, H. Sun, Z. Zhong, Smart polymersomes dually functionalized with cRGD and fusogenic GALA peptides enable specific and high-efficiency cytosolic delivery of apoptotic proteins, Biomacromolecules 20 (1) (2018) 184–191.
[30] S. Cao, Y. Xia, J. Shao, B. Guo, Y. Dong, I.A.B. Pijpers, Z. Zhong, F. Meng, L.K.E. A. Abdelmohsen, D.S. Williams, J.C.M. van Hest, Biodegradable polymersomes with structure inherent fluorescence and targeting capacity for enhanced photodynamic therapy, Angew. Chem. Int. Ed. 60 (32) (2021) 17629–17637.
[31] N.E. Donlon, R. Power, C. Hayes, J.V. Reynolds, J. Lysaght, Radiotherapy, immunotherapy, and the tumour microenvironment: turning an immunosuppressive milieu into a therapeutic opportunity, Cancer Lett. 502 (2021) 84–96.
[32] C. Wujanto, B. Vellayappan, S. Siva, A.V. Louie, M. Guckenberger, B.J. Slotman, H. Onishi, Y. Nagata, M. Liu, S.S. Lo, Stereotactic body radiotherapy for oligometastatic disease in non-small cell lung cancer, Front. Oncol. 9 (2019) 01219.
[33] S. Kaasa, E. Brenne, J.-A. Lund, P. Fayers, U. Falkmer, M. Holmberg, M. Lagerlund, O. Bruland, Prospective randomised multicenter trial on single fraction radiotherapy (8Gy×1) versus multiple fractions (3Gy×10) in the treatment of painful bone metastases, Radiother. Oncol. 79 (3) (2006) 278–284.
[34] R.T. Hoppe, C. Harrison, M. Tavallaee, S. Bashey, U. Sundram, S. Li, L. Million, B. Dabaja, P. Gangar, M. Duvic, Y.H. Kim, Low-dose total skin electron beam therapy as an effective modality to reduce disease burden in patients with mycosis fungoides: results of a pooled analysis from 3 phase-II clinical trials, J. Am. Acad. Dermatol. 72 (2) (2015) 286–292.
[35] K. Wallner, G. Merrick, L. True, T. Sherertz, S. Sutlief, W. Cavanagh, W. Butler, 20Gy versus 44Gy supplemental beam radiation with Pd-103 prostate brachytherapy: preliminary biochemical outcomes from a prospective randomized multi-center trial, Radiother. Oncol. 75 (3) (2005) 307–310.
[36] J. Stagg, E. Golden, E. Wennerberg, The interplay between the DNA damage response and ectonucleotidases modulates tumor response to therapy, Sci. Immunol. 8 (2023) eabq3015.
[37] K.E. de Visser, J.A. Joyce, The evolving tumor microenvironment: from cancer initiation to metastatic outgrowth, Cancer Cell 41 (3) (2023) 374–403.
[38] X. Yang, C. Shi, H. Li, S. Shen, C. Su, H. Yin, MARCH8 attenuates cGAS-mediated innate immune responses through ubiquitylation, Sci. Signal. 15 (2022) eabk3067.
[39] H. Bronger, J. Singer, C. Windmüller, U. Reuning, D. Zech, C. Delbridge, J. Dorn, M. Kiechle, B. Schmalfeldt, M. Schmitt, S. Avril, CXCL9 and CXCL10 predict

survival and are regulated by cyclooxygenase inhibition in advanced serous ovarian cancer, Brit. J. Cancer 115 (5) (2016) 553–563.
[40] G. van Loo, M.J.M. Bertrand, Death by TNF: a road to inflammation, Nat. Rev. Immunol. 23 (5) (2022) 289–303.
[41] S. Chen, A.F.U.H. Saeed, Q. Liu, Q. Jiang, H. Xu, G.G. Xiao, L. Rao, Y. Duo, Macrophages in immunoregulation and therapeutics, Signal Transduct. Target. Ther. 8 (1) (2023) 207.
[42] J. Zhang, D. Huang, P.E. Saw, E. Song, Turning cold tumors hot: from molecular mechanisms to clinical applications, Trends Immunol. 43 (7) (2022) 523–545.
[43] Y. Zhang, M.M. Rahman, P.A. Clark, R.N. Sriramaneni, T. Havighurst, C.P. Kerr, M. Zhu, J. Jones, X. Wang, K. Kim, S. Gong, Z.S. Morris, In situ vaccination following intratumoral injection of IL2 and poly-l-lysine/iron oxide/CpG nanoparticles to a radiated tumor site, ACS Nano 17 (11) (2023) 10236–10251.
[44] G. Cui, Y. Sun, L. Qu, C. Shen, Y. Sun, F. Meng, Y. Zheng, Z. Zhong, Uplifting antitumor immunotherapy with lymphnode-targeted and ratio-controlled codelivery of tumor cell lysate and adjuvant, Adv. Healthc. Mater. 13 (2024) 2303690.
[45] J. Liu, Y. Bai, Y. Li, X. Li, K. Luo, Reprogramming the immunosuppressive tumor microenvironment through nanomedicine: an immunometabolism perspective, eBioMedicine 107 (2024) 105301.
[46] Y. Su, W. Xu, Q. Wei, Y. Ma, J. Ding, X. Chen, Chiral polypeptide nanoparticles as nanoadjuvants of nanovaccines for efficient cancer prevention and therapy, Sci. Bull. 68 (3) (2023) 284–294.
[47] Y. Zhang, L. Liu, H. He, Y. Sun, Z. Zhong, Dual and multi-immune activation strategies for emerging cancer immunotherapy, Mater. Today 80 (2024) 406–428.
[48] L. Sun, F. Shen, L. Tian, H. Tao, Z. Xiong, J. Xu, Z. Liu, ATP-responsive smart hydrogel releasing immune adjuvant synchronized with repeated chemotherapy or radiotherapy to boost antitumor immunity, Adv. Mater. 33 (18) (2021) 2007910.
[49] Y. Chen, Y. Huang, Q. Li, Z. Luo, Z. Zhang, H. Huang, J. Sun, L. Zhang, R. Sun, D. J. Bain, J.F. Conway, B. Lu, S. Li, Targeting Xkr8 via nanoparticle-mediated in situ co-delivery of siRNA and chemotherapy drugs for cancer immunochemotherapy, Nat. Nanotechnol. 18 (2) (2022) 193–204.
[50] J. Zhao, Y. Xu, S. Ma, Y. Wang, Z. Huang, H. Qu, H. Yao, Y. Zhang, G. Wu, L. Huang, W. Song, Z. Tang, X. Chen, A minimalist binary vaccine carrier for personalized postoperative cancer vaccine therapy, Adv. Mater. 34 (10) (2022) 2109254.
[51] J.C. Jagodinsky, W.J. Jin, A.M. Bates, R. Hernandez, J.J. Grudzinski, I.R. Marsh, I. Chakravarty, I.S. Arthur, L.M. Zangl, R.J. Brown, E.J. Nystuen, S.E. Emma, C. Kerr, P.M. Carlson, R.N. Sriramaneni, J.W. Engle, E. Aluicio-Sarduy, T. E. Barnhart, T. Le, K. Kim, B.P. Bednarz, J.P. Weichert, R.B. Patel, Z.S. Morris, Temporal analysis of type 1 interferon activation in tumor cells following external beam radiotherapy or targeted radionuclide therapy, Theranostics 11 (13) (2021) 6120–6137.
[52] M.A. Miller, R. Chandra, M.F. Cuccarese, C. Pfirschke, C. Engblom, S. Stapleton, U. Adhikary, R.H. Kohler, J.F. Mohan, M.J. Pittet, R. Weissleder, Radiation therapy primes tumors for nanotherapeutic delivery via macrophage-mediated vascular bursts, Sci. Transl. Med. 9 (2017) eaal0225.
[53] T. Lammers, V. Subr, P. Peschke, R. Kühnlein, W.E. Hennink, K. Ulbrich, F. Kiessling, M. Heilmann, J. Debus, P.E. Huber, G. Storm, Image-guided and passively tumour-targeted polymeric nanomedicines for radiochemotherapy, Brit. J. Cancer 99 (6) (2008) 900–910.